nature medicine

ARTICLES

https://doi.org/10.1038/s41591-019-0668-z

A selective BCL-X_L PROTAC degrader achieves safe and potent antitumor activity

Sajid Khan[1,10], Xuan Zhang[2,10], Dongwen Lv[1,10], Qi Zhang[3], Yonghan He[1], Peiyi Zhang[2], Xingui Liu[1], Dinesh Thummuri[1], Yaxia Yuan[1], Janet S. Wiegand[1], Jing Pei[1], Weizhou Zhang[4], Abhisheak Sharma[5], Christopher R. McCurdy[2], Vinitha M. Kuruvilla[3], Natalia Baran[3], Adolfo A. Ferrando[6], Yong-mi Kim[7], Anna Rogojina[8], Peter J. Houghton[8], Guangcun Huang[9], Robert Hromas[9], Marina Konopleva[3], Guangrong Zheng[2,11*] and Daohong Zhou[1,11*]

B-cell lymphoma extra large (BCL-X_L) is a well-validated cancer target. However, the on-target and dose-limiting thrombocytopenia limits the use of BCL-X_L inhibitors, such as ABT263, as safe and effective anticancer agents. To reduce the toxicity of ABT263, we converted it into DT2216, a BCL-X_L proteolysis-targeting chimera (PROTAC), that targets BCL-X_L to the Von Hippel-Lindau (VHL) E3 ligase for degradation. We found that DT2216 was more potent against various BCL-X_L-dependent leukemia and cancer cells but considerably less toxic to platelets than ABT263 in vitro because VHL is poorly expressed in platelets. In vivo, DT2216 effectively inhibits the growth of several xenograft tumors as a single agent or in combination with other chemotherapeutic agents, without causing appreciable thrombocytopenia. These findings demonstrate the potential to use PROTAC technology to reduce on-target drug toxicities and rescue the therapeutic potential of previously undruggable targets. Furthermore, DT2216 may be developed as a safe first-in-class anticancer agent targeting BCL-X_L.

The evasion of apoptosis is a key hallmark of cancer[1], which is in part attributable to the overexpression of anti-apoptotic proteins in the BCL-2 family, including BCL-2, BCL-X_L and myeloid cell leukemia 1 (MCL-1)[2,3]. Inhibition of these BCL-2 family proteins with small molecules has been extensively investigated as a therapeutic strategy for cancers[4–9], resulting in the discovery of ABT263 (navitoclax, a BCL-2 and BCL-X_L dual inhibitor), ABT199 (venetoclax, a BCL-2 selective inhibitor) and several BCL-X_L and MCL-1 monoselective inhibitors as promising anticancer drug candidates[10–16]. Currently, ABT199 is the only Food and Drug Administration (FDA)-approved antitumor agent targeting the BCL-2 family proteins[17,18]. ABT263 is not approved because inhibition of BCL-X_L induces on-target and dose-limiting thrombocytopenia[19–21].

Although ABT199 is useful for the treatment of certain hematological malignancies, such as chronic lymphocytic leukemia and acute myeloid leukemia, it has limited utility for the treatment of solid tumors[22–24], because most solid tumor cells are not dependent on BCL-2 for survival[23,24]. In contrast, BCL-X_L is predominantly overexpressed in many solid tumor cells and also in a subset of leukemia cells[23,24], and its expression is highly correlated with resistance to cancer therapy, independent of a person's tumor protein P53 (*TP53*, also known as *P53*) mutational status[25,26]. To date, BCL-X_L stands as one of the most important validated cancer targets without a safe and effective therapeutic. In this context, development of a platelet-sparing BCL-X_L-targeting agent has the potential to transform the treatment of BCL-X_L-dependent malignancies.

PROTACs are bivalent small molecules containing a ligand that recognizes the target protein linked to an E3 ligase ligand. Such molecules can recruit the target protein to the E3 ligase, promote proximity-induced ubiquitination of the target protein and lead to its degradation through the ubiquitin proteasome system (UPS). PROTACs act catalytically to induce protein degradation in a substoichiometric manner. Their effect is not limited by equilibrium occupancy, and therefore requires less total drug exposure[27–31]. They generally have longer-acting activity but reduced toxicity compared with typical occupancy-driven protein inhibitors and are increasingly being used to develop more effective antitumor agents[32–38]. More importantly, because PROTACs rely on E3 ligases to induce protein degradation, they can achieve cell and/or tissue selectivity even when their target proteins are ubiquitously expressed. They achieve this by targeting the proteins to an E3 ligase that is differentially expressed in tumor cells compared with normal tissues. Therefore, we hypothesized that PROTAC technology can be exploited to reduce the thrombocytopenia induced by BCL-X_L inhibition, by converting a BCL-X_L inhibitor into a BCL-X_L PROTAC that targets BCL-X_L to an E3 ligase that is minimally expressed in platelets. Here we report the first proof-of-concept evidence to our knowledge using PROTAC technology to generate a cell-selective BCL-X_L PROTAC, termed DT2216, which has improved antitumor activity but reduced platelet toxicity compared with ABT263. This is achieved by targeting BCL-X_L to the Von Hippel-Lindau (VHL) E3 ligase, which is minimally expressed in platelets. In addition,

[1]Department of Pharmacodynamics, University of Florida, Gainesville, FL, USA. [2]Department of Medicinal Chemistry, College of Pharmacy, University of Florida, Gainesville, FL, USA. [3]Department of Leukemia, University of Texas M.D. Anderson Cancer Center, Houston, TX, USA. [4]Department of Pathology, Immunology and Laboratory Medicine, College of Medicine, University of Florida, Gainesville, FL, USA. [5]Department of Pharmaceutics, College of Pharmacy, University of Florida, Gainesville, FL, USA. [6]Department of Pediatrics, Pathology, Cell Biology and Systems of Biology and Institute for Cancer Genetics, Columbia University, New York, NY, USA. [7]Department of Pediatrics, Children's Hospital Los Angeles, Los Angeles, CA, USA. [8]Greehey Children's Cancer Research Institute, University of Texas Health Science Center at San Antonio, San Antonio, TX, USA. [9]Department of Medicine, the Long School of Medicine, University of Texas Health Science Center at San Antonio, San Antonio, TX, USA. [10]These authors contributed equally: Sajid Khan, Xuan Zhang, Dongwen Lv. [11]These authors jointly supervised this work: Guangrong Zheng, Daohong Zhou. *e-mail: zhengg@cop.ufl.edu; zhoudaohong@cop.ufl.edu

DT2216 does not degrade BCL-2, yet can synergistically kill a variety of cancer cells that are not solely dependent on BCL-X_L for survival when combined with a BCL-2 inhibitor, an MCL-1 inhibitor or a chemotherapeutic agent. These findings support the potential of DT2216 to be developed as a safe first-in-class BCL-X_L-targeting antitumor agent. More broadly, our results define a new general strategy to convert antitumor agents with on-target tissue-specific and dose-limiting toxicities to tumor-selective, less toxic PROTACs by engaging a tumor- or tissue/cell-specific E3 ligase.

Results

DT2216 has increased antitumor activity but reduced platelet toxicity. By analyzing human platelet RNA-sequencing data, we identified VHL as an E3 ligase minimally expressed in human platelets[39,40]. We confirmed this finding by immunoblotting, which showed that VHL expression was barely detectable in platelets. However, high levels of expression of VHL and BCL-X_L were detected in multiple human tumor cells, with the exception of VHL-null 786-O renal cell carcinoma (RCC) cell line (Extended Data Fig. 1a,b). This was consistent with high levels of *VHL* and BCL2 like 1 (*BCL2L1*) mRNA expression in a variety of human malignancies, as we analyzed using The Cancer Genome Atlas (TCGA) database (Extended Data Fig. 1c)[41,42]. On the basis of this finding, we rationally designed and synthesized a series of BCL-X_L PROTACs that target BCL-X_L to VHL for ubiquitination and degradation by linking the BCL-2/BCL-X_L binding moiety (BCL-2/X_L-L) derived from ABT263 to a VHL ligand (VHL-L) (Fig. 1a and Extended Data Fig. 1d). In addition, a BCL-X_L PROTAC negative control (DT2216NC) compound that cannot bind to VHL was synthesized as a control. Among these BCL-X_L PROTACs, DT2216 was selected as a lead because of its high potency in inducing BCL-X_L degradation in MOLT-4 T-cell acute lymphoblastic leukemia (T-ALL) cells with the half-maximal degradation concentration (DC_{50}) of 63 nM and maximum degradation (D_{max}) of 90.8% (Fig. 1b). Notably, we observed minimal reduction (D_{max}, 26%) in BCL-X_L levels in platelets after incubation with up to 3 μM of DT2216 (Fig. 1c). The induction of BCL-X_L degradation by DT2216 in MOLT-4 cells was rapid and long lasting (Extended Data Fig. 2a,b). Because both MOLT-4 cells and platelets are solely dependent on BCL-X_L for survival[19,24,43], we next evaluated the effects of DT2216 on the viability of MOLT-4 cells and platelets in comparison with ABT263. As previously reported, ABT263 was highly toxic to both MOLT-4 cells and platelets (Fig. 1d)[24,43]. In contrast, DT2216 (half-maximal effective concentration (EC_{50}), 0.052 μM) was about fourfold more cytotoxic to MOLT-4 cells than ABT263 (EC_{50}, 0.191 μM), and exerted almost no effect on the viability of platelets up to a concentration of 3 μM (Fig. 1d). Both DT2216 and ABT263 killed MOLT-4 cells by caspase-3-mediated induction of apoptosis in a BCL-2 homologous antagonist killer (BAK)- and BCL-2-associated X protein (BAX)-dependent manner (Fig. 1e–h and Extended Data Fig. 2c,d). However, ABT263 functions as a BCL-X_L inhibitor that inhibits the interaction of BCL-X_L with BAK, BAX and BIM indiscriminately in both MOLT-4 cells and platelets, whereas DT2216 acts as a BCL-X_L PROTAC that degrades BCL-X_L selectively in MOLT-4 cells but not in platelets (Fig. 1i,j). These findings confirm that DT2216 is a BCL-X_L PROTAC that has improved antitumor potency and reduced toxicity to platelets compared with ABT263.

DT2216 induces proteasomal degradation of BCL-X_L via VHL. To further confirm that DT2216 degrades BCL-X_L via VHL and proteasome, we first examined the effects of ABT263 and VHL-L alone and in combination on BCL-X_L levels in MOLT-4 cells and found that none of these treatments affected the levels of BCL-X_L (Fig. 2a). In addition, we found that preincubation of MOLT-4 cells with an excess amount of ABT263 or VHL-L inhibited the formation of the BCL-X_L–DT2216–VHL ternary complex (Extended Data Fig. 3a) and DT2216-induced BCL-X_L degradation (Fig. 2b,c). However, DT2216 had no effect on the levels of BCL-X_L in VHL-null 786-O renal cell carcinoma (RCC) cells (Fig. 2d). Furthermore, DT2216NC, which lacks VHL binding, failed to form the BCL-X_L–DT2216–VHL ternary complex (Extended Data Fig. 3b) and degrade BCL-X_L (Fig. 2e), and inhibition of proteasome activity with MG132 abolished the degradation of BCL-X_L induced by DT2216 (Fig. 2f). Moreover, the effect of DT2216 on MOLT-4 cell viability was also dependent on its PROTAC activity because VHL-L alone was not cytotoxic to the cells, and it did not have any additive or synergistic effect on MOLT-4 cell viability when combined with ABT263 (Fig. 2g), but it did reduce the cytotoxicity of DT2216 (Fig. 2h). Finally, DT2216NC showed no cytotoxicity against MOLT-4 cells (Fig. 2i). Collectively, these data confirm that DT2216 acts as a PROTAC that depends on the VHL E3 ligase and proteasomes to degrade BCL-X_L and induce apoptosis in MOLT-4 cells.

DT2216 is a specific BCL-X_L PROTAC. ABT263 has a high binding affinity for BCL-X_L and BCL-2 but binds more weakly to other members in the BCL-2 family, such as BCL-W or MCL-1 (Extended Data Fig. 4a)[13,24]. The binding affinities of DT2216 for BCL-X_L, BCL-2 and BCL-W were all reduced by about seven- to ninefold compared with that of ABT-263, but those for BCL-X_L and BCL-2 remained high. To investigate the ability of DT2216 to degrade not only BCL-X_L, but also BCL-2 and other anti-apoptotic BCL-2 family members, we selected tumor cell lines that express high levels of BCL-X_L, BCL-2, BCL-W and/or MCL-1 (Fig. 3a and Extended Data Fig. 4b,c). Our analyses revealed that DT2216 selectively degraded BCL-X_L, but did not change the levels of BCL-2 in all cells examined even though it has a higher binding affinity for BCL-2 than BCL-X_L. In addition, DT2216 had no effect on the levels of BCL-W and MCL-1 in these cells (Fig. 3b and Extended Data Fig. 4b,c). These findings are in agreement with the observations that DT2216 exhibited an eightfold reduction in its potency against RS4 B-cell ALL cells, which primarily depend on BCL-2 for survival, compared with ABT263 (ref. [24]) (Extended Data Fig. 4d and Supplementary Table 1). DT2216 was also not cytotoxic to MCL-1-dependent H929 myeloma cells[16] (Extended Data Fig. 4e and Supplementary Table 1). To further validate the specificity of DT2216, we used the stable-isotope labeling with amino acids in cell culture (SILAC) and liquid chromatography–tandem mass spectrometry (LC–MS/MS)-based proteomics to analyze the changes in proteins in cells after DT2216 and DT2216NC treatment (Extended Data Fig. 4f). The SILAC and LC–MS/MS results show that DT2216, but not DT2216NC, reduced the levels of BCL-X_L, but both agents did not affect expression of any other proteins (Fig. 3c), demonstrating that DT2216 is a specific BCL-X_L PROTAC. The lack of BCL-2 degradation by BCL-X_L PROTACs is not unique to DT2216, because the other BCL-X_L PROTAC we synthesized that is similar to DT2216, but targets a different E3 ligase (such as cereblon), degraded BCL-X_L but not BCL-2 (Extended Data Fig. 4g).

The selectivity of a PROTAC is largely determined by its ability to form a stable and cooperative ternary complex with its targeted protein(s) and E3 ligase[44,45]. To elucidate the mechanism of selectivity of DT2216, we first measured the formation of the BCL-2– or BCL-X_L–DT2216–VHL ternary complexes in vitro using the AlphaLISA assay[44]. These analyses revealed that both BCL-2 and BCL-X_L can form stable ternary complexes with DT2216 and VHL in cell-free conditions (Fig. 3d,e). However, only BCL-X_L, but not BCL-2, seems to be able to form stable ternary complexes with DT2216 and VHL in live cells, as determined by nanoBRET assay, a bioluminescence resonance energy transfer (BRET)-based assay to measure the interaction of two binding proteins in live cells[46] (Fig. 3f), even though both proteins could bind to DT2216 in a cellular thermal-shift assay (Extended Data Fig. 4h). These results are consistent with the ability of DT2216 to selectively induce BCL-X_L, but not BCL-2,

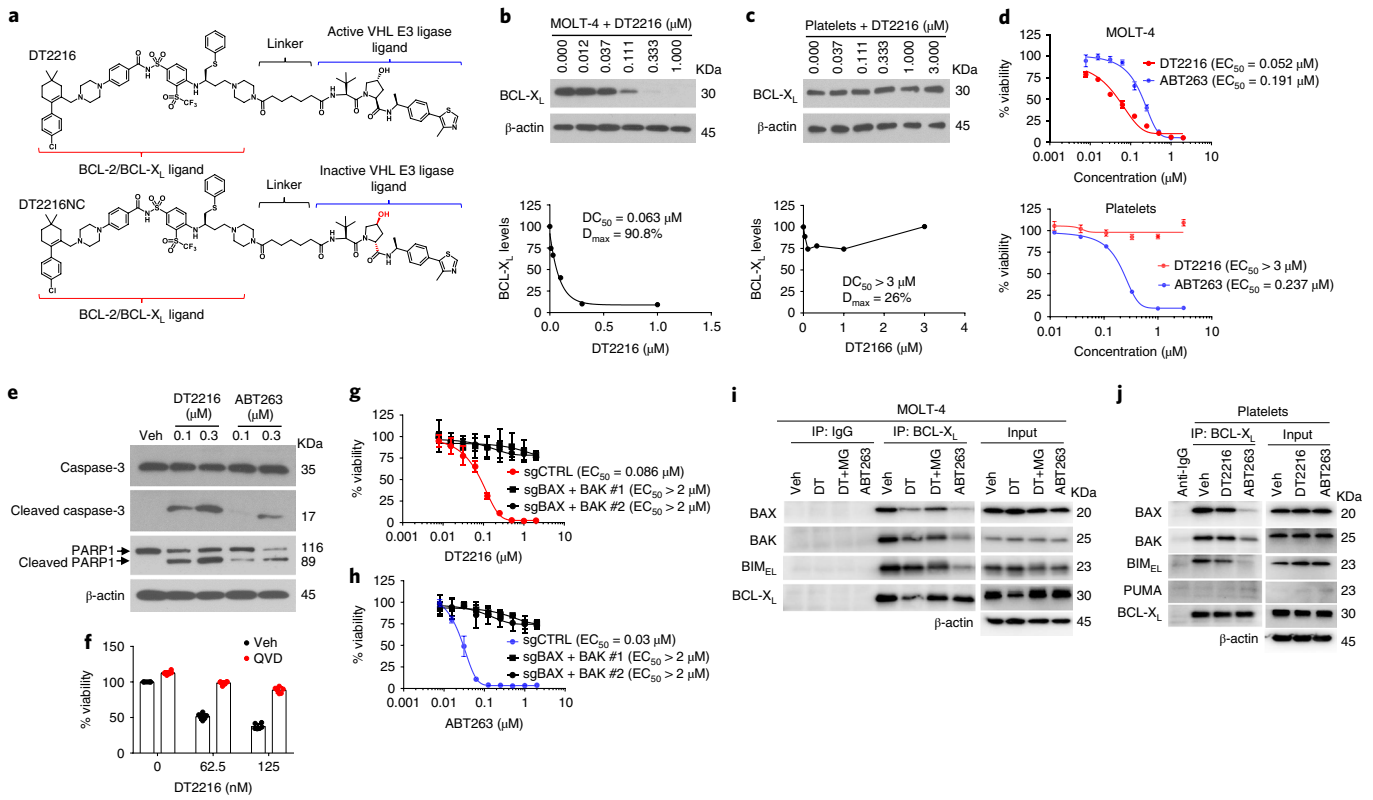

Fig. 1 | DT2216, a BCL-X$_L$ PROTAC, selectively induces BCL-X$_L$ degradation and apoptosis in BCL-X$_L$-dependent MOLT-4 T-ALL cells but not in platelets. **a**, Chemical structures of DT2216 and negative-control DT2216NC showing a dual BCL-2 and BCL-X$_L$ ligand (BCL-2/BCL-X$_L$ ligand) linked to a VHL ligand via an optimized linker. DT2216NC has the inactive VHL ligand that does not bind to VHL. **b**,**c**, DT2216 selectively degrades BCL-X$_L$ in MOLT-4 cells (**b**) but not in platelets (**c**) after treatment with increasing concentrations of DT2216 as indicated for 16 h. Top, Representative immunoblot. Bottom, Densitometric analyses of BCL-X$_L$ expression. Data points represent the mean ($n = 2$ and 3 independent experiments for MOLT-4 and platelets, respectively). DC$_{50}$, the drug concentration causing 50% protein degradation; D$_{max}$, the maximum level of degradation. **d**, Viability of MOLT-4 cells and human platelets were determined after they were incubated with increasing concentrations of DT2216 and ABT263 for 72 h. The data are presented as mean ± s.d. from six and three replicate cell cultures in a representative experiment for MOLT-4 and platelets, respectively. Similar results were also observed in two additional independent experiments. For the platelet-viability assay, each experiment used platelets from one individual donor. EC$_{50}$ values are the average of three independent experiments. **e**, A representative of two independent immunoblot analyses of cleaved and full-length caspase-3 and poly(ADP-ribose) polymerase 1 (PARP1) in MOLT-4 cells 24 h after they were treated with vehicle (Veh), DT2216 or ABT263. **f**, Cell viability of MOLT-4 cells was determined after the cells were pretreated with the pan-caspase inhibitor Q-VD-OPh (QVD, 10 μM) and were then treated with DT2216 for 72 h at the indicated concentrations. Data are presented as mean ± s.d. from six replicate cell cultures in a representative experiment. Each symbol represents data from an individual replicate. Similar results were also observed in one additional independent experiment. **g**,**h**, Viability of non-targeting small guide RNA (sgRNA)-transfected (sgCTRL) and *BAX* and *BAK* (*BAK1*) double-knockout (KO; represented as sgBAX + BAK) H146 cells was determined after cells were incubated with increasing concentrations of DT2216 or ABT263 for 72 h. Data are presented as mean ± s.d. from three replicate cell cultures in a representative experiment. Similar results were also observed in one additional independent experiment. **i**,**j**, MOLT-4 cells and human platelets were treated with either DT2216 (DT, 1 μM) or ABT263 (1 μM) for 6 h. MOLT-4 cells were pretreated with MG132 (MG, 1 μM) for 1 h in order to block BCL-X$_L$ degradation. Immunoblots of BAX, BAK and BH3-only pro-apoptotic proteins, BIM-extra large (BIM$_{EL}$) and PUMA, after immunoprecipitation with BCL-X$_L$ and in whole-cell lysates (Input) are shown from a single experiment. β-actin was used as an equal loading control in all immunoblot analyses shown in **b**, **c**, **e**, **i** and **j**. The uncropped immunoblot images related to this figure are provided in separate source data file.

ubiquitination and subsequent degradation by proteasomes (Fig. 3g) and are in agreement with previous reports demonstrating that the specificity of a PROTAC can be determined in part by its ability to form ternary complexes with its target proteins[44,45]. The differential formation of ternary complexes in vitro and in cell may be attributable to numerous factors, including the inherent differences between these two assays. For example, the full-length BCL-X$_L$ and BCL-2 were expressed in cells for the nanoBRET assay, whereas recombinant-transmembrane-domain-deleted proteins were used for the AlphaLISA assay. In addition, some other proteins may interfere with the interaction between BCL-2, DT2216 and VHL in live cells. However, the exact reason for the limited capacity of DT2216 to form ternary complexes with BCL-2 in cells is not known at this point and would be an important topic for future research.

Inspection of BCL-X$_L$–ABT263 X-ray crystal structures (protein data bank (PDB) entry: 4QNQ) (Fig. 3h)[14] revealed Lys 16, Lys 20, Lys 87 and Lys 157 in BCL-X$_L$ as solvent-exposed residues and potential ubiquitination sites. The conformations of other two lysine residues (Lys 205 and Lys 233) are not resolved, probably because they are buried in the transmembrane region of mitochondria, which precludes them from being potential ubiquitination sites[47]. Analyses of BCL-X$_L$ mutants with a lysine-to-arginine substitution revealed that DT2216 can degrade Flag-tagged wild-type BCL-X$_L$ and the K157R mutant, but not the BCL-X$_L$ mutants with all lysines mutated to arginines or with a K87R or K87H single mutant (Fig. 3i,j). These results support the notion that K87 is required for the degradation of BCL-X$_L$ by DT2216. Consistently, only K87-ubiquinated BCL-X$_L$ could be detected in DT2216-treated cells by proteomics. Moreover,

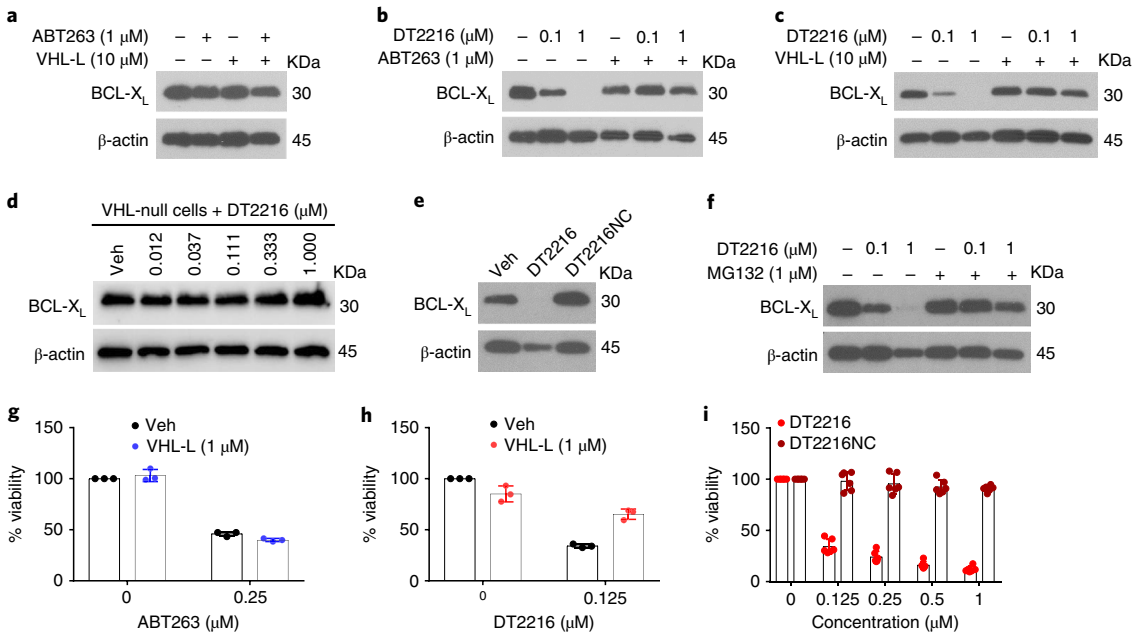

Fig. 2 | DT2216 degrades BCL-X_L in a VHL- and proteasome-dependent manner. a, ABT263 and/or VHL-L cannot induce BCL-X_L degradation in MOLT-4 cells. An immunoblot analysis of BCL-X_L in MOLT-4 cells is shown after the cells were treated with ABT263, VHL-L or the combination of both for 16 h. **b**, Pretreatment with ABT263 blocks BCL-X_L degradation by DT2216. An immunoblot analysis of BCL-X_L in MOLT-4 cells after the cells were either left untreated or pretreated with ABT263 for 1 h and then were treated with or without DT2216 as indicated for 16 h. **c**, Pretreatment with VHL-L blocks the BCL-X_L degradation by DT2216. An immunoblot analysis of BCL-X_L in MOLT-4 cells is shown. The cells were either left untreated or pretreated with VHL-L for 1 h and then were treated with or without DT2216 as indicated for 16 h before being assayed. **d**, An immunoblot analysis of BCL-X_L in VHL-null 786-O cells treated with vehicle or increasing concentrations of DT2216 for 16 h. **e**, An immunoblot analysis of BCL-X_L in MOLT-4 cells is shown. The cells were treated with 1 μM of DT2216 and its negative control DT2216NC for 16 h before being assayed. **f**, Proteasome inhibition blocks the BCL-X_L degradation by DT2216. A representative of two immunoblot analyses of BCL-X_L in MOLT-4 cells after they were either left untreated or pretreated with the proteasome inhibitor MG132 for 1 h, and then were treated with or without DT2216 for 16 h. **g**, Cell viability of MOLT-4 cells treated with or without ABT263 in the presence or absence of VHL-L for 72 h. **h**, Cell viability of MOLT-4 cells after they were either left untreated or pretreated with VHL-L for 1 h, and then were treated with DT2216 for 72 h. The data presented in **g** and **h** are mean ± s.d. from three replicate cell cultures in one representative experiment. Each symbol represents data from an individual replicate. Similar results were obtained in an additional independent experiment. **i**, Cell viability of MOLT-4 cells after treatment with increasing concentrations of DT2216 or its negative control DT2216NC for 72 h. The data represent mean ± s.d. from six replicate cell cultures in one representative experiment. Each symbol represents data from an individual replicate. Similar results were obtained in one additional independent experiment. β-actin was used as an equal loading control in immunoblot analyses shown in **a**–**f**. The uncropped immunoblot images related to this figure are provided in separate source data file.

BCL-X_L that only retains Lys 87 (K87-only, that is all the lysines are mutated to arginines except Lys 87) could be degraded by DT2216 (Fig. 3j,k). These findings suggest that DT2216 degrades BCL-X_L in a Lys 87-ubiquitination-dependent manner, which is in agreement with a recent report indicating that the formation of a ternary complex is necessary but not sufficient for a PROTAC to induce its target ubiquitination and degradation[48].

DT2216 is a more potent and safer antitumor agent than ABT263 in vivo. DT2216 is metabolically stable and has a favorable pharmacokinetic property for in vivo study via either intraperitoneal (i.p.) or intravenous (i.v.) injection, but is not bioavailable by oral (per os, p.o.) administration (Extended Data Fig. 5a–c and Supplementary Tables 2 and 3). A single dose of i.p. injection of DT2216 at 15 mg per kg body weight produced an intratumoral concentration of DT2216 in MOLT-4 T-ALL xenografts significantly greater than the cellular EC_{50} values of DT2216 for the cells for more than one week, which led to a sustained reduction in BCL-X_L expression (Fig. 4a,b, Extended Data Fig. 5d,e and Supplementary Table 4). Next, we examined the effects of different doses of DT2216 on platelet levels in mice in comparison with the therapeutically equivalent doses of ABT263; DT2216 is about fourfold more potent than ABT263 against MOLT-4 cells in vitro (Fig. 1d)[13]. ABT263 doses ranging from 25 to 100 mg per kg body weight caused severe thrombocytopenia in mice after 6 h of administration (Fig. 4c), which raises the risk of spontaneous hemorrhage as reported previously[49]. Platelet count gradually recovered 3 d after ABT263 administration and then exceeded the normal value thereafter, before coming back to the normal level 10 d after the treatment. This rebound can potentially increase the risk of thrombosis[50]. In contrast, platelet counts after treatment with DT2216 were mildly reduced and were not followed by reactive thrombocytosis (Fig. 4c). These results demonstrate that, at therapeutically equivalent doses, DT2216 is less toxic to platelets than ABT263 in mice.

Dose-escalation studies showed that DT2216 after weekly administration at 15 mg per kg body weight was more effective at suppressing the growth of MOLT-4 T-ALL xenografts in mice than 7.5 mg per kg body weight DT2216 was (Extended Data Fig. 6a–c). We next compared the effects of repeated treatments with DT2216 (15 mg per kg body weight, every 7 d (q7d), i.p.) and ABT263 (50 mg per kg body weight, qd, p.o.) on blood platelet counts and MOLT-4 T-ALL xenograft growth (Fig. 4d–g and Extended Data Fig. 7). In these analyses, daily ABT263 treatment induced severe and persistent thrombocytopenia with only moderate effects on MOLT-4 T-ALL xenograft growth as shown previously[13]. In contrast, once weekly dosing of DT2216 almost completely inhibited MOLT-4

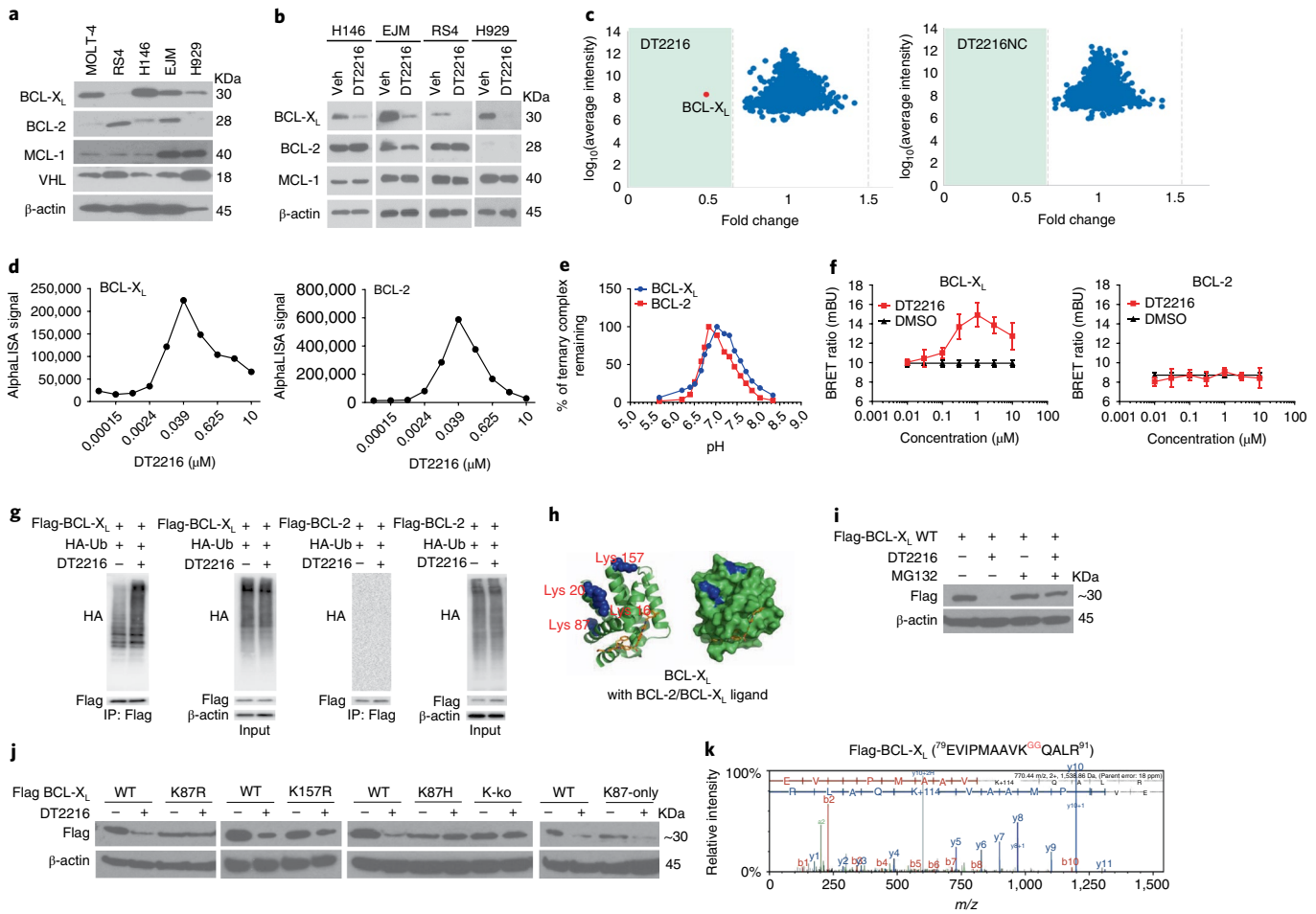

Fig. 3 | DT2216 is a BCL-X_L-specific PROTAC and induces BCL-X_L degradation through Lys 87 ubiquitination. a, A representative of two immunoblot analyses of BCL-X_L, BCL-2, MCL-1 and VHL in distinct tumor cell lines. **b**, A representative immunoblot analysis of BCL-X_L, BCL-2 and MCL-1 in H146 SCLC cells after they were treated with 0.1 μM DT2216 for 48 h, and in RS4 B-ALL cells and EJM and H929 multiple myeloma cells after they were treated with 1 μM DT2216 for 16 h. Similar results were obtained in one additional independent experiment. **c**, Proteomic analysis showing specificity of DT2216 for BCL-X_L degradation in comparison with its negative-control DT2216NC in WI-38 cells. **d**, Ternary complex formation of BCL-X_L or BCL-2 with DT2216 and VHL, determined by AlphaLISA assay. Data are expressed as the mean of a single experiment ($n = 2$ technical replicates). Similar results were obtained in two more independent assays performed with BCL-X_L. **e**, pH stability of the ternary complex formed by DT2216 and the VHL complex and BCL-X_L or BCL-2, as measured by AlphaLISA assay. Data are expressed as mean ($n = 2$ technical replicates). Similar results were obtained in one additional independent experiment. **f**, NanoBRET ternary complex formation of BCL-X_L and BCL-2. Ternary complex formation was determined in 293T cells after they transiently expressed HiBit-BCL-X_L, LgBit and HaloTag-VHL or HiBit-BCL-2, LgBit and HaloTag-VHL and were then treated with a serial dilution of DT2216. Data are expressed as mean ± s.e.m. of three independent experiments. **g**, Representative immunoblot of hemagluttinin (HA), Flag and β-actin following Flag immunoprecipitation of protein extracts from 293T cells that were cotransfected as indicated with Flag-BCL-X_L and HA-tagged ubiquitin (HA-Ub) or Flag-BCL-2 and HA-ubiquitin plasmids, and then were treated with or without DT2216 (1 μM) and MG132 (10 μM) as indicated for 4 h. Data are representative of three independent experiments. **h**, Crystal structure of BCL-X_L with ABT263 (BCL-2/BCL-X_L ligand). The lysines are colored blue. **i**, A representative immunoblot analysis of BCL-X_L showing that DT2216 induces wild-type (WT) BCL-X_L degradation in a proteasome-dependent manner. Flag-BCL-X_L-WT plasmid was transfected into 293T cells for 40 h, and then the cells were treated with or without DT2216 (1 μM) and MG132 (10 μM) as indicated for 6 h. Similar results were obtained in two more independent experiments. **j**, Representative immunoblot analysis of BCL-X_L showing that DT2216 induces BCL-X_L degradation dependent on Lys 87 ubiquitination. For the analysis, Flag-BCL-X_L-WT and the K87R and K157R (lysine to arginine), K87H (lysine to histidine), K-ko (all the lysines in BCL-X_L were mutated to arginines) and K87-only (all the lysines in BCL-X_L were mutated to arginines except Lys 87) Flag-BCL-X_L mutant plasmids were transfected into 293 T cells for 40 h, and then the cells were treated with or without 1 μM DT2216 for 6 h. Similar results were obtained in two more independent experiments. **k**, Lys 87 is the only ubiquitination site triggered by DT2216. 293T cells were co-transfected with Flag-BCL-X_L and HA-ubiquitin vectors. Extracts were immunoprecipitated with anti-Flag affinity resin, followed by trypsin and AspN digestion and tandem mass spectrometry, as described in the Methods. A fragmentation spectrum of ubiquitinated EVIPMAAVKQALR peptide (ubiquitinated Lys 87 residue) of BCL-X_L. The parent ion corresponding to this peptide has been subjected to higher-energy collisional dissociation in mass spectrometer. The detected b- and y-fragment ion series have been labeled. The results were obtained from a single experiment. β-actin was used as equal loading control in immunoblotting experiments shown in **a**, **b**, **g**, **i** and **j**. The uncropped immunoblot images related to this figure are provided in separate source data file.

T-ALL xenograft growth with only moderate and transient reduction in platelet counts and no significant change in body weight. MOLT-4 T-ALL xenografts progressing under ABT263 treatment at a lower dose level (15 mg per kg body weight, q7d, i.p.) that did not cause severe thrombocytopenia, effectively responded to treatment with DT2216 (15 mg per kg body weight, q4d, i.p.) without

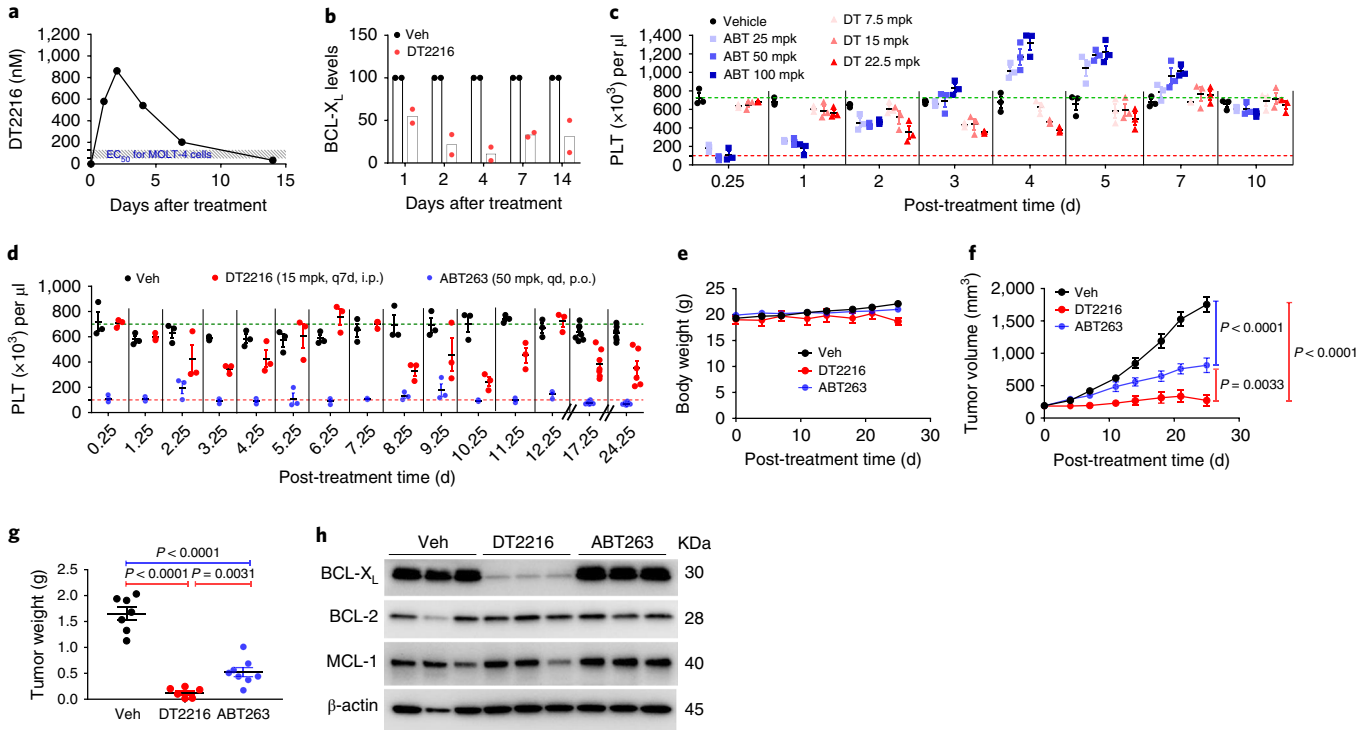

Fig. 4 | DT2216 is more potent against MOLT-4 T-ALL xenografts and less toxic to platelets than ABT263 in mice. a, Concentration of DT2216 in MOLT-4 tumors after a single DT2216 administration (15 mg per kg body weight/i.p.). Data represent the average of two mice in a group at each time point. **b**, Densitometric analysis of BCL-X_L protein levels in tumors (mean, $n=2$ mice in a group at each time point) at different durations after a single vehicle or DT2216 administration (15 mg per kg body weight, i.p.). Each symbol represents data (% of vehicle) from an individual animal. The representative immunoblots are shown in Extended Data Fig. 5e. **c**, Numeration of platelets (PLT) 0.25, 1, 2, 3, 4, 5, 7 and 10 d after a single i.p. injection with DT2216 or p.o. dosing with ABT263 at the indicated doses. Data are represented as mean ± s.e.m. ($n=3$ mice in each group). Each symbol represents data from an individual animal. mpk, mg per kg body weight. **d**, Numeration of platelets after the mice were continuously treated with DT2216 or ABT263 as indicated. Data are represented as mean ± s.e.m. ($n=3$ mice in each group until day 12.25; $n=7$ mice in vehicle, 7 mice in DT2216 and 8 mice in ABT263 at day 17.25; $n=7$ mice in vehicle, 6 mice in DT2216 and 8 mice in ABT263 at day 24.25). Each symbol represents data from an individual animal. In **c** and **d**, the green and red dashed lines indicate average platelet count in vehicle-treated mice and platelet count at or below which, respectively, there is an increased risk of hemorrhage. **e**,**f**, Body-weight and tumor-volume changes in mice after the start of treatment with vehicle, DT2216 (15 mg per kg body weight, q7d, i.p.) or ABT263 (50 mg per kg body weight, qd, p.o.). Data presented are mean ± s.e.m. ($n=7$ mice in vehicle, 7 mice in DT2216 and 8 mice in ABT263 at the start of treatment). Statistical significance was determined by two-sided unpaired Student's *t*-test. **g**, MOLT-4 tumor-bearing mice were euthanized 25 d after treatment initiation (4 d and 1 d after last dose of DT2216 and ABT263, respectively). Tumor weights at the end of study are shown. Data are presented as mean ± s.e.m. ($n=7$ mice in vehicle, 6 mice in DT2216 and 8 mice in ABT263). Each symbol represents data from an individual animal, and the middle horizontal line represents the mean. Statistical significance was determined by two-sided unpaired Student's *t*-test. **h**, Immunoblot analysis of BCL-X_L, BCL-2 and MCL-1 in MOLT-4 tumors ($n=3$ mice in each group). The uncropped immunoblot images related to this figure are provided in a separate source data file.

significant changes in body weight and blood platelet counts (Extended Data Fig. 8a–f). The potent antitumor activity of DT2216 was correlated with its ability to induce BCL-X_L degradation (Fig. 4h). These findings support that DT2216 is a safer and more potent antitumor agent than ABT263. It also demonstrated that DT2216 has the potential to be used as a single agent to treat tumors solely dependent on BCL-X_L.

Synergy of DT2216 in combination with BCL-2 or MCL-1 inhibitors. Hematological and solid tumors frequently engage more than one member of the BCL-2 family proteins for survival[24,51,52]. For example, NCI-H146 (H146) human small-cell lung cancer (SCLC) cells are dependent on both BCL-X_L and BCL-2 for survival, whereas EJM myeloma cells depend on MCL-1 and BCL-X_L for survival[16] (Fig. 5a,b and Supplementary Table 1). Inhibition of BCL-2 and MCL-1 with their respective inhibitors ABT199 and S63845 had moderate effects on the viability of H146 and EJM cells, respectively. However, their effect was significantly augmented by the addition of DT2216, resulting in synergistic killing of both cell lines (Fig. 5a,b).

Next, we examined whether DT2216 can be combined with ABT199 to more effectively eradicate tumors dependent on both BCL-X_L and BCL-2, such as H146 SCLC xenografts, than ABT263 can (Fig. 5c). Treatment of H146 SCLC xenografts with DT2216, ABT199, ABT263 and DT2216 plus ABT199 induced no significant changes in body weight (Fig. 5d). Administration of DT2216 at 15 mg per kg body weight per week by i.p. injection alone or in combination with ABT199 at 50 mg per kg body weight per day by p.o. administration did not cause any significant reduction in platelet levels, whereas i.p. administration of 15 mg per kg body weight per week of ABT263 did (Fig. 5e). Treatment with DT2216, ABT199 or ABT263 alone significantly inhibited tumor growth, resulting in 81.6%, 57.9% and 59.5% mean tumor growth inhibition (TGI) at the end of the experiment (Fig. 5f,g and Extended Data Fig. 9), respectively. Moreover, the combination of DT2216 and ABT199 induced markedly increased antitumor effects resulting in almost complete suppression of tumor growth (mean 98.2% TGI). The TGI induced by DT2216 was also associated with a significant reduction in BCL-X_L expression in the tumors harvested at the end of DT2216 treatment (Fig. 5h). These findings suggest that DT2216 can be

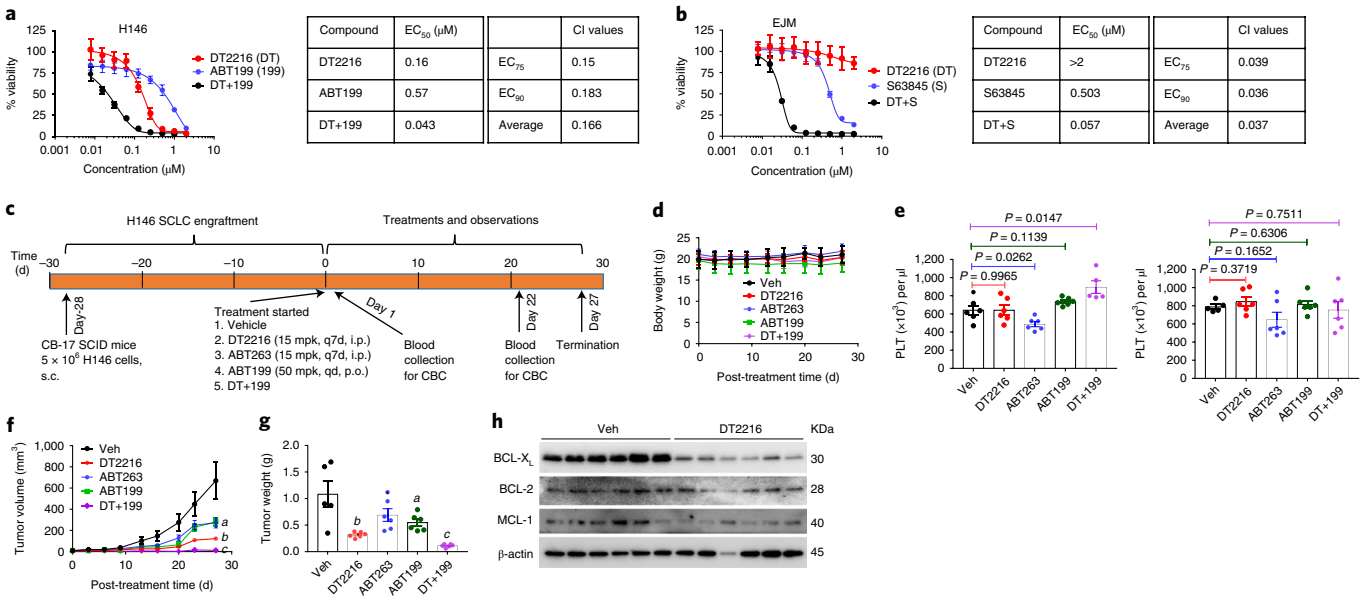

Compound	EC_{50} (μM)		CI values
DT2216	0.16	EC_{75}	0.15
ABT199	0.57	EC_{90}	0.183
DT+199	0.043	Average	0.166

Compound	EC_{50} (μM)		CI values
DT2216	>2	EC_{75}	0.039
S63845	0.503	EC_{90}	0.036
DT+S	0.057	Average	0.037

Fig. 5 | Synergy of DT2216 with other BCL-2 family protein inhibitors. a, Percentage of viable H146 SCLC cells after 72 h treatment with increasing concentrations of DT2216 (DT) and ABT199 (199, a BCL-2 specific inhibitor) alone or the combination of these two at equimolar concentrations (1:1) as indicated is presented in the graph on the left. EC_{50} values for each of these treatments, the combination index (CI) at EC_{75} and EC_{90} values, and the average CI are presented in the table on the right. Data are presented as mean ± s.d. from six replicate cell cultures in one representative experiment. Similar results were obtained in one additional independent experiment. **b**, Percentage of viable EJM multiple myeloma cells after 72 h treatment with increasing concentrations of DT2216 (DT) and S63845 (S, a MCL-1 specific inhibitor) alone or the combination of these two at equimolar concentrations (1:1) is presented in the graph on the left. EC_{50} values for each of these treatments, CI at EC_{75} and EC_{90} values, and the average CI are presented in the table. Data are presented as mean ± s.d. from six replicate cell cultures in one representative experiment. Similar results were obtained in one additional independent experiment. **c**, Illustration of the experimental design of H146 SCLC xenograft model. **d**, Body weight changes in H146 SCLC tumor-bearing mice after the start of treatment with vehicle, DT2216, ABT263 or ABT199 alone or the combination of DT2216 (DT) and ABT199 (199) as shown in **c**. Data are presented as mean ± s.e.m. ($n = 6$ mice per group at the start of treatment). **e**, Blood platelets were numerated 1 d after first treatment with all the agents (left), and 1 d after last treatment with DT2216 or ABT263 and 22nd dose of ABT199 (right) as shown in **c**. Data are presented as mean ± s.e.m. ($n = 5$ mice each for DT+199 in the left graph and vehicle in the right graph, $n = 6$ mice each in other groups). Each symbol represents data from an individual animal. Statistical significance was determined by two-sided unpaired Student's *t*-test. **f**, Changes in tumor volume over time after the start of treatment as shown in **c**. Data are presented as mean ± s.e.m. ($n = 6$ mice per group at the start of treatment). *a* ($P = 0.0381$ ABT263 versus vehicle, $P = 0.0400$ ABT199 versus vehicle); *b* ($P = 0.0069$ versus vehicle, $P = 0.0152$ versus ABT263, $P = 0.0044$ versus ABT199); and *c* ($P = 0.0022$ versus vehicle, $P = 0.0001$ versus DT2216, $P = 0.0003$ versus ABT263, $P < 0.0001$ versus ABT199) determined by two-sided unpaired Student's *t*-test at post-treatment day 27. **g**, The average wet weight of excised tumors from each group. Data are presented as mean ± s.e.m. ($n = 5$ mice in vehicle, and 6 mice each in other groups). Each symbol represents data from an individual animal. *a* ($P = 0.0524$ versus vehicle); *b* ($P = 0.0086$ versus vehicle, $P = 0.0116$ versus ABT263, $P = 0.0072$ versus ABT199); and *c* ($P = 0.002$ verus vehicle, $P < 0.0001$ versus DT2216, $P = 0.0006$ versus ABT263, $P < 0.0001$ versus ABT199) determined by two-sided unpaired Student's *t*-test. **h**, A representative of two immunoblot analyses of BCL-X_L BCL-2 and MCL-1 in the H146 SCLC tumors excised at the end of experiment ($n = 6$ mice in each group). β-actin was used as a loading control. The uncropped immunoblot images related to this figure are provided in separate source data file.

combined with ABT199 to more effectively treat tumors dependent on both BCL-X_L and BCL-2 than either agent alone or ABT263, without causing significant platelet toxicity. Of note, the combination of DT2216 and S63845, a selective MCL-1 inhibitor, was lethal to mice because the liver cells are also dependent on both BCL-X_L and MCL-1 for survival[53], which limits the use of this combination as a systemic therapy to treat cancer.

Synergy between DT2216 and conventional chemotherapy. High levels of BCL-X_L expression are associated with chemotherapy resistance across multiple tumor types[25,26], and inhibition of BCL-X_L with ABT263 can improve the therapeutic efficacy of various chemotherapeutic agents[24,54,55]. However, the on-target thrombocytopenia resulting from BCL-X_L inhibition prevents the use of combination therapy of ABT263 with other cytotoxic chemotherapeutic agents in clinic[24,54,55]. To evaluate the potential of DT2216 to overcome chemoresistance, we evaluated the ability of this agent to enhance the effects of chemotherapy. In these experiments, DT2216 sensitized drug-resistant triple-negative MDA-MB-231 breast cancer (BC) cells to docetaxel, doxorubicin and vincristine in vitro (Fig. 6a). A similar chemosensitizing effect was also observed in PC-3 prostate, HepG2 liver and SW620 colon cancer cells (Supplementary Table 5), but not in 786-O RCC cells (Fig. 6b), which lack VHL expression (Fig. 2d and Extended Data Fig. 1b).

To determine whether DT2216 can sensitize MDA-MB-231 BC cells to docetaxel in vivo, we generated MDA-MB-231 BC xenografts in mice and then treated the mice with vehicle, docetaxel and/or DT2216 as shown in Fig. 6c. We found that DT2216 alone had minimal effect on tumor growth, while docetaxel was able to substantially inhibit it. However, the combination of docetaxel and DT2216 was more effective at suppressing the tumor growth than docetaxel alone without causing significant changes in body weight (Fig. 6d,e).

Patient-derived xenograft (PDX) tumor models can better recapitulate tumor biology of human diseases than conventional tumor xenograft models employing cancer cell lines can. They are also more predictive of clinical outcomes of experimental therapeutic agents than the latter[56]. Therefore, we used CUL76 T-ALL PDX to

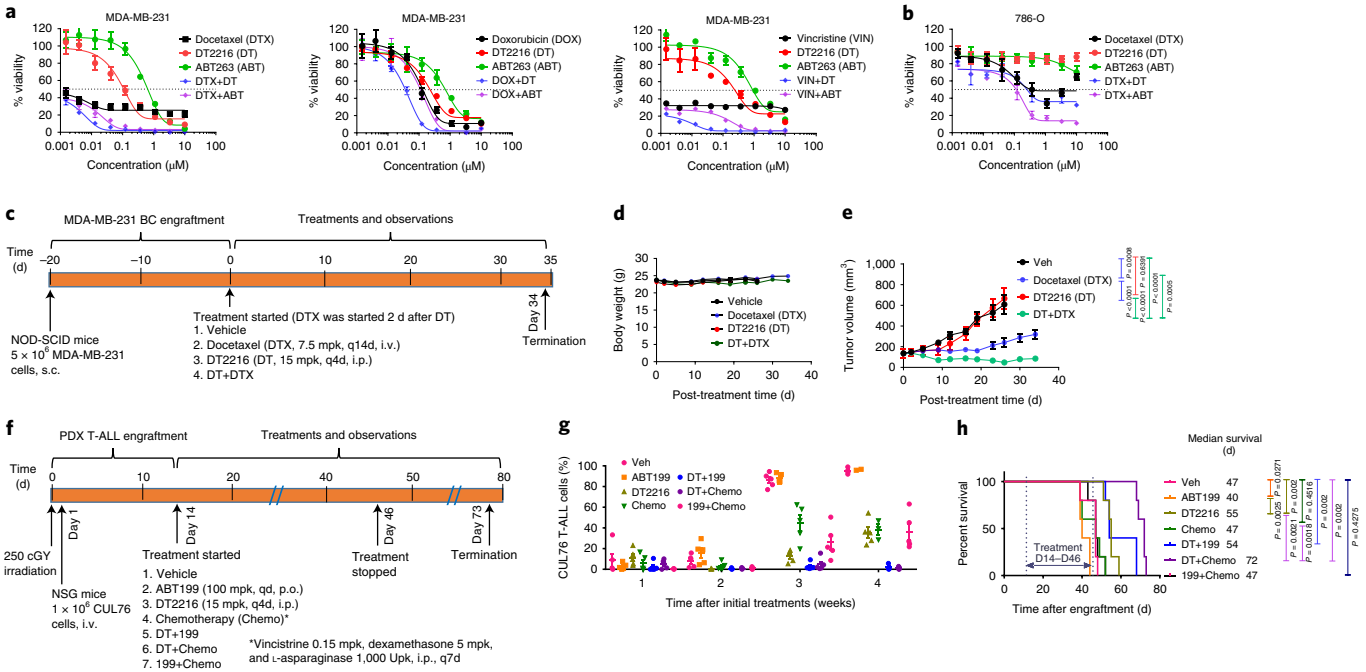

Fig. 6 | Synergy of DT2216 with chemotherapy. a, Percentage of viable MDA-MB-231 triple-negative breast cancer cells after 72 h of treatment with increasing concentrations of DT2216, ABT263, docetaxel (DTX), doxorubicin (DOX) or vincristine (VIN) alone or the combination of DT2216 (DT) or ABT263 (ABT) with one of the chemotherapeutic agents. Data are presented as mean ± s.d. from three replicate cell cultures in one representative experiment. Similar results were obtained in two additional independent experiments for DTX. **b**, Percentage of viable VHL-null 786-O renal cell carcinoma cells after 72 h treatment with docetaxel (DTX), DT2216 or ABT263 alone, or the combination of DT2216 (DT) or ABT263 (ABT) with DTX as indicated. Data are presented as mean ± s.d. from three replicate cell cultures of a single experiment. For the combination treatment, cells were treated with an equimolar ratio of two drugs (1:1), except the combination of DTX with DT2216 or ABT263 in MDA-MB-231 cells, where the ratios of DTX and DT2216 or ABT263 were 1:10. **c**, Illustration of the experimental design of MDA-MB-231 breast cancer xenograft model. **d**,**e**, Body weight and tumor volume changes in MDA-MB-231 tumor-bearing mice after the start of treatment with vehicle, DTX, DT2216 or the combination of these two as shown in **c**. Data are presented as mean ± s.e.m. ($n = 10$ mice in each group at the start of treatment). Statistical significance was determined by two-sided unpaired Student's *t*-test at post-treatment day 26. **f**, Illustration of the experimental design of CUL76 T-ALL PDX model. Upk, units per kilogram body weight. **g**, Percentage of CUL76 T-ALL cells in mouse blood collected at various times after the initiation of the treatments as shown in **f**. Data are presented as mean ± s.e.m. ($n = 5$ mice in each group at the start of treatment). Each symbol represents data from an individual animal, and the middle horizontal line represents the mean. **h**, Kaplan–Meier survival curve showing the survival of mice after CUL76 T-ALL engraftment. Median survival time within each treatment group is presented along with statistical analysis results ($n = 5$ mice in each group at the start of treatment). Statistical significance was determined by log-rank (Mantel–Cox) test.

validate whether DT2216 can be combined with ABT199 or chemotherapy to more effectively inhibit the growth of tumor cells from people with relapsed or refractory T-ALL. CUL76 T-ALL PDX was highly resistant to conventional chemotherapy and expressed high levels of BCL-X_L, BCL-2 and MCL-1 (Fig. 6f and Supplementary Fig. 1a,c). This PDX grew rapidly after being transplanted into NOD-SCID IL2Rgnull (NSG) mice (Fig. 6g and Supplementary Fig. 1b). Mice with CUL76 T-ALL PDX had a median survival time of 47, 40 and 47 d after the initiation of treatments with vehicle, ABT199 and a standard T-ALL chemotherapy regimen consisting of vincristine, dexamethasone and L-asparaginase (VDL), respectively (Fig. 6h). Treatment with DT2216 alone or DT2216 plus ABT199 moderately prolonged the survival of the mice, whereas the combination of DT2216 with VDL chemotherapy substantially increased survival (Fig. 6h). The extension of survival correlated with reduced circulating tumor burden of CUL76 T-ALL cells serially measured by flow cytometry in the blood (Fig. 6g and Supplementary Fig. 1c). Similar results were also observed in two additional T-ALL PDX models (Extended Data Fig. 10a–d). These findings confirm that DT2216 can sensitize drug-resistant tumor cells to chemotherapy in vivo.

Discussion

Here we report a novel strategy to reduce the on-target and dose-limiting normal tissue toxicity of an antitumor agent using PROTAC technology. Specifically, we show that we can convert a non-selective BCL-2 and BCL-X_L inhibitor that is highly toxic to platelets into a BCL-X_L-specific PROTAC with significantly reduced platelet toxicity. This was achieved by linking the BCL-2/BCL-X_L binding moiety derived from ABT263 to a VHL-L with an empirically optimized linker. The resulting BCL-X_L-specific PROTAC lead compound, DT2216, can selectively induce BCL-X_L degradation in various tumor cells, but not in platelets, because it targets BCL-X_L to the VHL E3 ligase that is minimally expressed in platelets.

These findings may have important clinical implications. First, BCL-X_L is a well-validated cancer target. However, the on-target and dose-limiting thrombocytopenia induced by BCL-X_L inhibition has limited the clinical use of BCL-X_L inhibitors[2,4,20,21]. By converting a BCL-2/BCL-X_L dual inhibitor into a BCL-X_L-specific PROTAC, we developed a safer and more effective BCL-X_L-targeting antitumor agent. Our lead BCL-X_L degrader, DT2216, significantly reduces the on-target and dose-limiting platelet toxicity resulting from conventional BCL-X_L inhibition. In addition, BCL-X_L-specific PROTACs should have another advantage compared to BCL-2/BCL-X_L dual inhibitors or BCL-X_L monoinhibitors, because PROTACs act catalytically to induce protein degradation in a substoichiometric manner, and their effect is not limited by equilibrium occupancy[27–31]. Therefore, it is not surprising that DT2216 is more potent than ABT263 in inducing tumor cell apoptosis in vitro and inhibiting

tumor growth in vivo. These findings suggest that DT2216 has greater clinical potential than ABT263 or other BCL-X_L inhibitors. However, it is unlikely that DT2216 will be totally devoid of platelet toxicity, because it retains a relatively reasonable binding affinity to BCL-X_L, and thus can still function as a moderate BCL-X_L inhibitor that could potentially induce mild thrombocytopenia if concentrations are high enough. Therefore, identifying effective and tolerable DT2216 doses and a schedule for administration will be an important task in future clinical-oncology trials.

Interestingly, while ABT263 inhibits both BCL-X_L and BCL-2, DT2216 is BCL-X_L-specific and does not induce BCL-2 degradation. In fact, proteomic analysis demonstrated that DT2216 is highly specific for BCL-X_L degradation. Similarly, the pan-bromodomain and extra-terminal (BET) inhibitor JQ1, which binds and inhibits the BET proteins bromodomain-containing protein 2 (BRD2), BRD3 and BRD4, has been converted into a selective BRD4 PROTAC[57]. Others have shown that a promiscuous ligand for multi-kinases could induce only a subset of its targets for degradation when converted into PROTACs[38,58]. As seen with other selective PROTACs reported previously, the lack of BCL-2 degradation by DT2216 is at least partially attributed to its inability to form a stable target protein–PROTAC–E3 ligase ternary complex in cells[44,45]. We anticipate that because DT2216 is a specific BCL-X_L PROTAC, it will have limited effect on cancers that depend on both BCL-X_L and BCL-2 for survival[24]. However, we showed that this hurdle can be overcome by combining DT2216 with other selective inhibitors of BCL-2 family proteins (such as ABT199) or with standard chemotherapy.

Our results present the proof of principle for the use of tissue-specific E3 ligases to direct tissue- or disease-specific degradation of a target protein using PROTAC technology. We demonstrate here that this strategy could rescue BCL-X_L as an anticancer target from its on-target and dose-limiting toxicity. This approach could also be applied to convert other toxic antitumor agents into tumor-selective PROTACs by engaging E3 ligases more abundantly expressed in tumor cells than in normal tissues.

Online content

Any methods, additional references, Nature Research reporting summaries, source data, extended data, supplementary information, acknowledgements, peer review information, details of author contributions and competing interests, and statements of code and data availability are available at https://doi.org/10.1038/s41591-019-0668-z.

Received: 11 February 2019; Accepted: 28 October 2019;
Published online: 02 December 2019

References

1. Hanahan, D. & Weinberg, R. A. Hallmarks of cancer: the next generation. *Cell.* **144**, 646–674 (2011).
2. Singh, R., Letai, A. & Sarosiek, K. Regulation of apoptosis in health and disease: the balancing act of BCL-2 family proteins. *Nat. Rev. Mol. Cell Biol.* **20**, 175–193 (2019).
3. Igney, F. H. & Krammer, P. H. Death and anti-death: tumour resistance to apoptosis. *Nat. Rev. Cancer* **2**, 277–288 (2002).
4. Ashkenazi, A., Fairbrother, W. J., Leverson, J. D. & Souers, A. J. From basic apoptosis discoveries to advanced selective BCL-2 family inhibitors. *Nat. Rev. Drug Discov.* **16**, 273–284 (2017).
5. Adams, J. M. & Cory, S. The Bcl-2 apoptotic switch in cancer development and therapy. *Oncogene* **26**, 1324–1337 (2007).
6. Reed, J. C. Bcl-2-family proteins and hematologic malignancies: history and future prospects. *Blood* **111**, 3322–3330 (2008).
7. Thomas, S. et al. Targeting the Bcl-2 family for cancer therapy. *Expert Opin. Ther. Targets* **17**, 61–75 (2013).
8. Opfermann, J. T. Attacking cancer's Achilles heel: antagonism of antiapoptotic BCL-2 family members. *FEBS J.* **283**, 2661–2675 (2016).
9. Garner, T. P., Lopez, A., Reyna, D. E., Spitz, A. Z. & Gavathiotis, E. Progress in targeting the BCL-2 family of proteins. *Curr. Opin. Chem. Biol.* **39**, 133–142 (2017).
10. Delbridge, A. R., Grabow, S., Strasser, A. & Vaux, D. L. Thirty years of BCL-2: translating cell death discoveries into novel cancer therapies. *Nat. Rev. Cancer* **16**, 99–109 (2016).
11. Delbridge, A. R. & Strasser, A. The BCL-2 protein family, BH3-mimetics and cancer therapy. *Cell Death Differ.* **22**, 1071–1080 (2015).
12. Oltersdorf, T. et al. An inhibitor of Bcl-2 family proteins induces regression of solid tumours. *Nature* **435**, 677–681 (2005).
13. Tse, C. et al. ABT-263: a potent and orally bioavailable Bcl-2 family inhibitor. *Cancer Res.* **68**, 3421–3428 (2008).
14. Souers, A. J. et al. ABT-199, a potent and selective BCL-2 inhibitor, achieves antitumor activity while sparing platelets. *Nat. Med.* **19**, 202–208 (2013).
15. Tao, Z. F. et al. Discovery of a potent and selective BCL-XL inhibitor with in vivo activity. *ACS Med. Chem. Lett.* **5**, 1088–1093 (2014).
16. Kotschy, A. et al. The MCL1 inhibitor S63845 is tolerable and effective in diverse cancer models. *Nature* **538**, 477–482 (2016).
17. Deeks, E. D. Venetoclax: first global approval. *Drugs* **76**, 979–987 (2016).
18. Roberts, A. W. et al. Targeting BCL2 with venetoclax in relapsed chronic lymphocytic leukemia. *N. Engl. J. Med.* **374**, 311–322 (2016).
19. Mason, K. D. et al. Programmed anuclear cell death delimits platelet life span. *Cell.* **128**, 1173–1186 (2007).
20. Schoenwaelder, S. M. et al. Bcl-xL-inhibitory BH3 mimetics can induce a transient thrombocytopathy that undermines the hemostatic function of platelets. *Blood* **118**, 1663–1674 (2011).
21. Kaefer, A. et al. Mechanism-based pharmacokinetic/pharmacodynamic meta-analysis of navitoclax (ABT-263) induced thrombocytopenia. *Cancer Chemother. Pharmacol.* **74**, 593–602 (2014).
22. Itchaki, G. & Brown, J. R. The potential of venetoclax (ABT-199) in chronic lymphocytic leukemia. *Adv. Hematol.* **7**, 270–287 (2016).
23. Perini, G. F., Ribeiro, G. N., Neto, J. V. P., Campos, L. T. & Hamerschlak, N. BCL-2 as therapeutic target for hematological malignancies. *J. Hematol. Oncol.* **11**, 65 (2018).
24. Leverson, J. D. et al. Exploiting selective BCL-2 family inhibitors to dissect cell survival dependencies and define improved strategies for cancer therapy. *Sci. Transl. Med.* **7**, 279ra40 (2015).
25. Amundson, S. A. et al. An informatics approach identifying markers of chemosensitivity in human cancer cell lines. *Cancer Res.* **60**, 6101–6110 (2000).
26. Vogler, M. Targeting BCL2-proteins for the treatment of solid tumours. *J. Adv Med.* **2014**, 943648 (2014).
27. Lai, A. C. & Crews, C. M. Induced protein degradation: an emerging drug discovery paradigm. *Nat. Rev. Drug Discov.* **16**, 101–114 (2017).
28. Runcie, A. C., Chan, K. H., Zengerle, M. & Ciulli, A. Chemical genetics approaches for selective intervention in epigenetics. *Curr. Opin. Chem. Biol.* **33**, 186–194 (2016).
29. Deshaies, R. J. Protein degradation: prime time for PROTACs. *Nat. Chem. Biol.* **11**, 634–635 (2015).
30. Churcher, I. Protac-induced protein degradation in drug discovery: breaking the rules or just making new ones? *J. Med. Chem.* **61**, 444–452 (2018).
31. Ohoka, N., Shibata, N., Hattori, T. & Naito, M. Protein knockdown technology: application of ubiquitin ligase to cancer therapy. *Curr. Cancer Drug Targets* **16**, 136–146 (2016).
32. Lu, J. et al. Hijacking the E3 ubiquitin ligase cereblon to efficiently target BRD4. *Chem. Biol.* **22**, 755–763 (2015).
33. Bondeson, D. P. et al. Catalytic in vivo protein knockdown by small-molecule PROTACs. *Nat. Chem. Biol.* **11**, 611–617 (2015).
34. Lai, A. C. et al. Modular PROTAC design for the degradation of oncogenic BCR-ABL. *Angew. Chem. Int. Ed.* **55**, 807–810 (2016).
35. Raina, K. et al. PROTAC-induced BET protein degradation as a therapy for castration-resistant prostate cancer. *Proc. Natl Acad. Sci. USA* **113**, 7124–7129 (2016).
36. Saenz, D. T. et al. Novel BET protein proteolysis-targeting chimera exerts superior lethal activity than bromodomain inhibitor (BETi) against post-myeloproliferative neoplasm secondary (s) AML cells. *Leukemia* **31**, 1951–1961 (2017).
37. Winter, G. E. et al. Drug development. Phthalimide conjugation as a strategy for in vivo target protein degradation. *Science* **348**, 1376–1381 (2015).
38. Huang, H. T. et al. A chemoproteomic approach to query the degradable kinome using a multi-kinase degrader. *Cell Chem. Biol.* **25**, 88–99.e6 (2018).
39. Bray, P. F. et al. The complex transcriptional landscape of the anucleate human platelet. *BMC Genomics* **14**, 1 (2013).
40. Kissopoulou, A., Jonasson, J., Lindahl, T. L. & Osman, A. Next generation sequencing analysis of human platelet PolyA$^+$ mRNAs and rRNA-depleted total RNA. *PLoS One* **8**, e81809 (2013).
41. Cerami, E. et al. The cBio cancer genomics portal: an open platform for exploring multidimensional cancer genomics data. *Cancer Discov.* **2**, 401–404 (2012).
42. Gao, J. et al. Integrative analysis of complex cancer genomics and clinical profiles using the cBioPortal. *Sci. Signal.* **6**, pl1 (2013).

43. Vogler, M. et al. BCL2/BCL-X(L) inhibition induces apoptosis, disrupts cellular calcium homeostasis, and prevents platelet activation. *Blood.* **117**, 7145–7154 (2011).
44. Gadd, M. S. et al. Structural basis of PROTAC cooperative recognition for selective protein degradation. *Nat. Chem. Biol.* **13**, 514–521 (2017).
45. Nowak, R. P. et al. Plasticity in binding confers selectivity in ligand-induced protein degradation. *Nat. Chem. Biol.* **14**, 706–714 (2018).
46. Riching, K. M. et al. Quantitative live-cell kinetic degradation and mechanistic profiling of PROTAC mode of action. *ACS Chem. Biol.* **13**, 2758–2770 (2018).
47. Farmer, T., O'Neill, K. L., Naslavsky, N., Luo, X. & Caplan, S. Retromer facilitates the localization of Bcl-xL to the mitochondrial outer membrane. *Mol. Biol. Cell* **30**, 1138–1146 (2019).
48. Smith, B. E. et al. Differential PROTAC substrate specificity dictated by orientation of recruited E3 ligase. *Nat. Commun.* **10**, 131 (2019).
49. Morowski, M. et al. Only severe thrombocytopenia results in bleeding and defective thrombus formation in mice. *Blood* **121**, 4938–4947 (2013).
50. Rinder, H. M. et al. Correlation of thrombosis with increased platelet turnover in thrombocytosis. *Blood* **91**, 1288–1294 (1998).
51. Koch, R. et al. Biomarker-driven strategy for MCL1 inhibition in T-cell lymphomas. *Blood* **133**, 566–575 (2018).
52. Berger, S. et al. Computationally designed high specificity inhibitors delineate the roles of BCL2 family proteins in cancer. *eLife.* **5**, e20352 (2016).
53. Hikita, H. et al. Mcl-1 and Bcl-xL cooperatively maintain integrity of hepatocytes in developing and adult murine liver. *Hepatology* **50**, 1217–1226.
54. Chen, J. et al. The Bcl-2/Bcl-X(L)/Bcl-w inhibitor, navitoclax, enhances the activity of chemotherapeutic agents in vitro and in vivo. *Mol. Cancer Ther.* **10**, 2340–2349 (2011).
55. Ackler, S. et al. The Bcl-2 inhibitor ABT-263 enhances the response of multiple chemotherapeutic regimens in hematologic tumors in vivo. *Cancer Chemother. Pharmacol.* **66**, 869–880 (2010).
56. Pompili, L., Porru, M., Caruso, C., Biroccio, A. & Leonetti, C. Patient-derived xenografts: a relevant preclinical model for drug development. *J. Exp. Clin. Cancer Res.* **35**, 189 (2016).
57. Zengerle, M., Chan, K. H. & Ciulli, A. Selective small molecule induced degradation of the BET bromodomain protein BRD4. *ACS Chem. Biol.* **10**, 1770–1777 (2015).
58. Bondeson, D. P. et al. Lessons in PROTAC design from selective degradation with a promiscuous warhead. *Cell Chem Biol.* **25**, 78–87.e5 (2018).

Methods

Chemical synthesis. The chemical structures and synthetic schemes for DT2216 and DT2216NC are presented in Extended Data Fig. 1d. Detailed synthetic procedures are provided below.

General methods. Tetrahydrofuran (THF), dichloromethane (DCM), toluene and acetonitrile were obtained via a solvent-purification system by filtration through two columns packed with activated alumina and a 4-Å molecular sieve, respectively. All other chemicals obtained from commercial sources were used without further purification. Flash chromatography was performed using silica gel (230–400 mesh) as the stationary phase. Reaction progress was monitored by thin-layer chromatography (silica-coated glass plates) and visualized by ultraviolet (UV) light, and/or by LC–MS. Nuclear magnetic resonance (NMR) spectra were recorded in $CDCl_3$ at 400 MHz for ^{1}H NMR. Chemical shifts (δ) are given in ppm using tetramethylsilane as an internal standard. Multiplicities of NMR signals are designated as singlet (s), broad singlet (br s), doublet (d), doublet of doublets (dd), triplet (t), quartet (q) and multiplet (m). All final compounds for biological testing were of ≥98.0% purity as analyzed by LC–MS, performed on an Advion AVANT LC system with the expression compact mass spectrometer using a Thermo Accucore Vanquish C18 + UHPLC Column (1.5 µm, 50 × 2.1 mm) at 40 °C. Gradient elution was used for UHPLC with a mobile phase of acetonitrile and water containing 0.1% formic acid.

Preparation of (R)-3-((tert-butoxycarbonyl)amino)-4-hydroxybutyric acid benzyl ester (compound 2). *N*-Methylmorpholine (4.41 ml, 40.1 mmol) and isobutyl chloroformate (4.43 ml, 34.2 mmol) were added into a stirred solution of *N*-Boc-D-aspartic acid 4-benzyl ester (compound 1) (10.0 g, 30.9 mmol) in THF (250 ml) at −25 °C. The resulting mixture was stirred at −25 °C for 30 min and allowed to warm to −15 °C. A solution of $NaBH_4$ (2.94 g, 77.7 mmol) in water (100 ml) was then added to the mixture in one portion resulting in evolution of gas. The mixture was stirred for 30 min at −15 °C and quenched with 1 N HCl (aq.). The solution was extracted with ethyl acetate three times, and the combined organic layers were washed with brine, dried over Na_2SO_4, filtered and evaporated to dryness under reduced pressure. The crude product was used directly in the next step. ^{1}H NMR (400 MHz, $CDCl_3$) δ 7.48–7.29 (m, 5H), 5.17 (br s, 1H), 5.12 (s, 2H), 4.05–3.93 (m, 1H), 3.69 (t, coupling constant (J) = 5.2 Hz, 2H), 2.67 (d, J = 6.1 Hz, 2H), 2.38 (br s, 1H), 1.42 (s, 9H). LC–MS (with electrospray ionization, ESI): *m/z* 310.3 $[M+H]^+$.

Preparation of benzyl (R)-3-((tert-butoxycarbonyl)amino)-4-(phenylthio)butanoate (compound 3). A mixture of compound 2 (30.9 mmol), diphenyl disulfide (8.8 g, 40.2 mmol) and Bu_3P (9.9 ml, 40.2 mmol) in toluene (150 ml) was heated at 80 °C under N_2 overnight. The mixture was cooled to room temperature and concentrated under reduced pressure. The crude product was purified by silica gel flash column chromatography using ethyl acetate and hexanes as eluents to afford the title compound (7.1 g, yield 57% in two steps). ^{1}H NMR (400 MHz, $CDCl_3$) δ 7.44–7.09 (m, 10H), 5.15 (br s, 1H), 5.08 (s, 2H), 4.24–3.97 (m, 1H), 3.23 (dd, J = 13.7, 5.5 Hz, 1H), 3.08 (dd, J = 13.6, 7.3 Hz, 1H), 2.80 (dd, J = 16.2, 5.1 Hz, 1H), 2.67 (dd, J = 16.4, 5.7 Hz, 1H), 1.40 (s, 9H). LC-MS (ESI): *m/z* 402.2 $[M+H]^+$.

Preparation of tert-butyl N-[(2R)-4-oxo-1-(phenylsulfanyl)butan-2-yl]carbamate (compound 4). Diisobutylaluminium hydride (DIBAL-H; 1.2 M in toluene, 34.0 ml, 40.8 mmol) was added dropwise to a solution of compound 3 (7.1 g, 17.7 mmol) in toluene (80 ml) at −78 °C and stirred for 3 h. The reaction mixture was then quenched with NH_4Cl (aq.), warmed to room temperature, and diluted with ethyl acetate. The resulting mixture was filtered, and the filtrate was poured into water and extracted with ethyl acetate. The combined organic phases were washed with brine, dried over Na_2SO_4, filtered and evaporated to dryness under reduced pressure. The crude product was purified by silica gel flash column chromatography using ethyl acetate and hexanes as eluents to afford the title compound (4.16 g, yield 80%). LC–MS (ESI): *m/z* 296.2 $[M+H]^+$.

Preparation of 2,2,2-trichloroethyl (R)-4-(3-((tert-butoxycarbonyl)amino)-4-(phenylthio)butyl)piperazine-1-carboxylate (compound 6). To a mixture of compound 4 (592 mg, 2.00 mmol), compound 5 (753 mg, 2.88 mmol) and triethylamine (TEA) (1.12 ml, 8.05 mmol) in DCM (15 ml) was added to $NaBH(OAc)_3$ (638 mg, 3.00 mmol). The resulting solution was stirred at room temperature overnight before being poured into water and extracted with DCM. The combined organic phases were washed with brine, dried over Na_2SO_4, filtered and evaporated to dryness under reduced pressure. The crude product was purified by silica gel flash column chromatography using ethyl acetate and hexanes as eluents to afford the title compound (733 mg, yield 68%). ^{1}H NMR (400 MHz, $CDCl_3$) δ 7.43–7.36 (m, 2H), 7.32–7.27 (m, 2H), 7.19 (t, J = 7.3 Hz, 1H), 5.44 (br s, 1H), 4.76 (s, 2H), 3.99–3.84 (m, 1H), 3.72–3.49 (m, 4H), 3.23 (dd, J = 13.3, 4.6 Hz, 1H), 3.10–2.95 (m, 1H), 2.61–2.31 (m, 6H), 1.96–1.61 (m, 2H), 1.43 (s, 9H). LC–MS (ESI): *m/z* 540.1 $[M+H]^+$.

Preparation of 2,2,2-trichloroethyl (R)-4-(3-amino-4-(phenylthio)butyl)piperazine-1-carboxylate trifluoroacetic acid salt (compound 7). To a mixture of compound 6 (733 mg, 1.36 mmol) in DCM (5 ml) was added to trifluoroacetic acid (TFA) (2.0 ml, 26.1 mmol). The mixture was stirred at room temperature for 1 h, and solvents were removed under reduced pressure. The solid residue was washed with diethyl ether to afford the title compound 7 (752 mg, yield 100%) as a white solid. ^{1}H NMR (400 MHz, $CDCl_3$): δ 7.41–7.33 (m, 2H), 7.31–7.26 (m, 2H), 7.23–7.15 (m, 1H), 4.74 (s, 2H), 3.73–3.41 (m, 4H), 3.20–2.66 (m, 5H), 2.58–2.28 (m, 6H), 1.84–1.57 (m, 2H). LC-MS (ESI): *m/z* 440.1 $[M+H]^+$.

Preparation of 2,2,2-trichloroethyl (R)-4-(4-(phenylthio)-3-((4-sulfamoyl-2-((trifluoromethyl)sulfonyl)phenyl)amino)butyl)piperazine-1-carboxylate (compound 9). A mixture of compounds 7 (752 mg, 1.36 mmol) and 8 (417 mg, 1.36 mmol) and TEA (945 µl, 6.80 mmol) in acetonitrile (20 ml) was stirred under reflux for 4 h. Solvents were evaporated under reduced pressure and the crude product was purified by silica gel flash column chromatography using ethyl acetate and hexanes as eluents to afford the title compound (780 mg, yield 79%) as a white solid. ^{1}H NMR (400 MHz, $CDCl_3$) δ 8.24 (d, J = 2.2 Hz, 1H), 7.84 (d, J = 9.1 Hz, 1H), 7.42–7.37 (m, 2H), 7.36–7.27 (m, 3H), 7.05 (d, J = 8.6 Hz, 1H), 6.65 (br s, 1H), 5.13 (br s, 2H), 4.76 (s, 2H), 4.02–3.88 (m, 1H), 3.75–3.40 (m, 4H), 3.16–2.97 (m, 2H), 2.82–2.26 (m, 6H), 2.19–2.05 (m, 1H), 1.85–1.77 (m, 1H). LC–MS (ESI): *m/z* 727.0 $[M+H]^+$.

Preparation of 2,2,2-trichloroethyl (R)-4-(3-((4-(N-(4-(4-((4′-chloro-4,4-dimethyl-3,4,5,6-tetrahydro-[1,1′-biphenyl]-2-yl)methyl)piperazin-1-yl)benzoyl)sulfamoyl)-2-((trifluoromethyl)sulfonyl)phenyl)amino)-4-(phenylthio)butyl)piperazine-1-carboxylate (compound 11). A mixture of compounds 9 (780 mg, 1.07 mmol) and 10 (470 mg, 1.07 mmol), 1-ethyl-3-(3-dimethylaminopropyl)carbodiimide (EDCI) (411 mg, 2.14 mmol) and 4-dimethylaminopyridine (DMAP) (262 mg, 2.14 mmol) in DCM (40 ml) was stirred at room temperature overnight. Solvent was evaporated under reduced pressure, and the crude product was purified by silica gel flash column chromatography using DCM and methanol (MeOH) as eluents to afford the title compound (859 mg, yield 70%) as a white solid. ^{1}H NMR (400 MHz, $CDCl_3$) δ 8.37 (d, J = 2.0 Hz, 1H), 8.13 (d, J = 9.2 Hz, 1H), 7.62 (d, J = 8.9 Hz, 2H), 7.41–7.27 (m, 6H), 7.12 (d, J = 8.7 Hz, 1H), 6.98 (d, J = 8.3 Hz, 2H), 6.79 (d, J = 9.0 Hz, 2H), 6.58 (d, J = 9.4 Hz, 1H), 4.75 (s, 2H), 3.95–3.81 (m, 1H), 3.63–3.38 (m, 4H), 3.33–3.23 (m, 4H), 3.11 (dd, J = 13.8, 4.9 Hz, 1H), 3.00 (dd, J = 13.9, 7.5 Hz, 1H), 2.81 (s, 2H), 2.46–2.01 (m, 15H), 1.75–1.65 (m, 1H), 1.46 (t, J = 6.3 Hz, 2H), 0.98 (s, 6H) ppm. LC–MS (ESI): *m/z* 1,147.1 $[M+H]^+$.

Preparation of (R)-4-(4-((4′-chloro-4,4-dimethyl-3,4,5,6-tetrahydro-[1,1′-biphenyl]-2-yl)methyl)piperazin-1-yl)-N-((4-((1-(phenylthio)-4-(piperazin-1-yl)butan-2-yl)amino)-3-((trifluoromethyl)sulfonyl)phenyl)sulfonyl)benzamide (compound 12). Zinc powder (960 mg, 14.8 mmol) was added to a mixture of compound 11 (316 mg, 0.28 mmol) and acetic acid (600 µl, 10.5 mmol) in THF (20 ml). The reaction mixture was stirred at room temperature for 5 h. The solid was removed by filtration, and the filtrate was poured into water and extracted with ethyl acetate. The combined organic phases were washed with brine, dried over Na_2SO_4, filtered and evaporated to dryness under reduced pressure. The crude product was purified by silica gel flash column chromatography using DCM, methanol and TEA as eluents to afford the title compound (210 mg, yield 78%). ^{1}H NMR (400 MHz, $CDCl_3$) δ 8.21 (s, 1H), 7.93 (d, J = 9.2 Hz, 1H), 7.85 (d, J = 8.6 Hz, 2H), 7.33–7.24 (m, 2H), 7.22–7.08 (m, 5H), 6.92 (d, J = 8.3 Hz, 2H), 6.77 (d, J = 8.4 Hz, 1H), 6.66 (d, J = 8.7 Hz, 2H), 6.46 (d, J = 9.3 Hz, 1H), 3.83–3.67 (m, 1H), 3.17–3.08 (m, 4H), 3.02–2.92 (m, 5H), 2.89–2.78 (m, 1H), 2.72 (s, 2H), 2.64–2.13 (m, 12H), 2.04–1.91 (m, 3H), 1.62–1.49 (m, 1H), 1.39 (t, J = 6.3 Hz, 2H), 0.91 (s, 6H) ppm. LC–MS (ESI): *m/z* 973.2 $[M+H]^+$.

Preparation of ethyl 7-(((S)-1-((2S,4R)-4-hydroxy-2-(((S)-1-(4-(4-methylthiazol-5-yl)phenyl)ethyl)carbamoyl)pyrrolidin-1-yl)-3,3-dimethyl-1-oxobutan-2-yl)amino)-7-oxoheptanoate (compound 15a). Compounds 13a and 13b were prepared according to reported procedures in the literature[35]. A mixture of compound 13a (100 mg, 0.207 mmol), 7-ethoxy-7-oxoheptanoic acid (compound 14) (44 mg, 0.234 mmol), HATU (82 mg, 0.216 mmol) and TEA (160 µl, 1.15 mmol) in DCM was stirred at room temperature for 1 h. The reaction mixture was poured into water and extracted with DCM. The combined organic layers were washed with aq. NH_4Cl solution and saline, dried over Na_2SO_4, and concentrated under vacuum. The crude product was purified by silica gel column chromatography to afford the title compound (105 mg, yield 83%). ^{1}H NMR (400 MHz, $CDCl_3$) δ 8.68 (s, 1 H), 7.50–7.32 (m, 5H), 6.26 (d, J = 8.7 Hz, 1H), 5.14–5.03 (m, 1H), 4.72 (t, J = 7.9 Hz, 1H), 4.59–4.46 (m, 2H), 4.14–4.08 (m, 3H), 3.61 (dd, J = 11.3, 3.7 Hz, 1H), 2.57–2.45 (m, 4H), 2.32–2.18 (m, 4H), 2.11–2.05 (m, 1H), 1.66–1.58 (m, 4H), 1.48 (d, *J* = 6.9 Hz, 3H), 1.36–1.22 (m, 5H), 1.04 (s, 9H) ppm. LC–MS (ESI): *m/z* 615.4 $[M+H]^+$.

Preparation of ethyl 7-(((S)-1-((2R,4S)-4-hydroxy-2-(((S)-1-(4-(4-methylthiazol-5-yl)phenyl)ethyl)carbamoyl)pyrrolidin-1-yl)-3,3-dimethyl-1-oxobutan-2-yl)amino)-7-oxoheptanoate (compound 15b). Compound 15b was prepared using the procedure described for the synthesis of compound 15a by using compound 13b instead of compound 13a. Yield 80%. ^{1}H NMR (400 MHz, $CDCl_3$) δ 8.65 (s, 1H), 7.35 (d, J = 9.2 Hz, 5H), 6.13–6.03 (m, 1H), 5.11–5.00 (m, 1H), 4.68 (dd, J = 8.5, 3.8 Hz, 1H), 4.55–4.44 (m, 1H), 4.33 (d, *J* = 7.1 Hz, 1H), 4.13–4.04 (m, 3H), 3.59 (dd, J = 10.4, 5.3 Hz, 1H), 2.51 (s, 3H), 2.47–2.38 (m, 1H), 2.27–2.15 (m, 4H), 2.11–2.01 (m, 1H),

1.62–1.53 (m, 4H), 1.40 (d, J = 7.0 Hz, 3H), 1.32–1.19 (m, 5H), 1.06 (s, 9H) ppm. LC–MS (ESI): *m/z* 615.5 $[M+H]^+$.

Preparation of (2S,4R)-1-((S)-2-(7-(4-((R)-3-((4-(N-(4-(4-((4′-chloro-4,4-dimethyl-3,4,5,6-tetrahydro-[1,1′-biphenyl]-2-yl)methyl)piperazin-1-yl)benzoyl)sulfamoyl)-2-((trifluoromethyl)sulfonyl)phenyl)amino)-4-(phenylthio)butyl)piperazin-1-yl)-7-oxoheptanamido)-3,3-dimethylbutanoyl)-4-hydroxy-N-((S)-1-(4-(4-methylthiazol-5-yl)phenyl)ethyl)pyrrolidine-2-carboxamide (DT2216). Compound 15a (105 mg, 0.171 mmol) was dissolved in methanol (5 ml) and treated with LiOH monohydrate (43 mg, 1.02 mmol) in water (0.5 ml) for 2 h. The pH of the reaction mixture was slowly adjusted to 5–6 with 1.0 N HCl. The mixture was concentrated directly under reduced pressure to afford the corresponding acid, which was dissolved in DCM (5 ml) and mixed with compound 12 (158 mg, 0.162 mmol), HATU (68 mg, 0.179 mmol) and TEA (113 µL, 0.810 mmol). The resulting solution was stirred at room temperature for 1 h before being poured into water and extracted with DCM. The combined organic layers were washed with NH_4Cl solution (aq.) and saline, dried over Na_2SO_4, and concentrated under reduced pressure. The crude product was purified by silica gel flash column chromatography to afford DT2216 (115 mg, yield 46%). ^{1}H NMR (400 MHz, $CDCl_3$) δ 8.67 (s, 1H), 8.34 (d, J = 2.3 Hz, 1H), 8.08 (d, J = 9.1 Hz, 1H), 7.69 (d, J = 8.6 Hz, 2H), 7.46–7.27 (m, 12H), 7.14–6.93 (m, 3H), 6.76 (d, J = 8.6 Hz, 2H), 6.61 (d, J = 9.4 Hz, 1H), 6.34 (d, J = 8.7 Hz, 1H), 5.13–5.00 (m, 1H), 4.79–4.69 (m, 1H), 4.60 (d, J = 8.7 Hz, 1H), 4.49 (s, 1H), 4.10 (d, J = 11.4 Hz, 1H), 3.96–3.83 (m, 1H), 3.72–2.81 (m, 13H), 2.55–2.00 (m, 24H), 1.77–1.30 (m, 12H), 1.03 (s, 9H), 0.97 (s, 6H) ppm. LC–MS (ESI): *m/z* 1,542.0 $[M+H]^+$.

Preparation of (2R,4S)-1-((S)-2-(7-(4-((R)-3-((4-(N-(4-(4-((4′-chloro-4,4-dimethyl-3,4,5,6-tetrahydro-[1,1′-biphenyl]-2-yl)methyl)piperazin-1-yl)benzoyl)sulfamoyl)-2-((trifluoromethyl)sulfonyl)phenyl)amino)-4-(phenylthio)butyl)piperazin-1-yl)-7-oxoheptanamido)-3,3-dimethylbutanoyl)-4-hydroxy-N-((S)-1-(4-(4-methylthiazol-5-yl)phenyl)ethyl)pyrrolidine-2-carboxamide (DT2216NC). DT2216NC was prepared using the procedure described for the synthesis of DT2216 by using compound 15b instead of compound 15a. Yield 40%. ^{1}H NMR (400 MHz, $CDCl_3$) δ 8.65 (s, 1H), 8.36 (d, J = 1.9 Hz, 1H), 8.11–8.04 (m, 1H), 7.69 (d, J = 8.8 Hz, 2H), 7.44–7.26 (m, 12H), 7.08 (d, J = 8.5 Hz, 1H), 6.98 (d, *J* = 8.3 Hz, 2H), 6.76 (d, J = 9.0 Hz, 2H), 6.62 (d, J = 9.4 Hz, 1H), 6.17 (d, J = 6.9 Hz, 1H), 5.13–5.02 (m, 1H), 4.68 (dd, J = 8.5, 3.9 Hz, 1H), 4.54–4.44 (m, 1H), 4.34 (d, J = 6.9 Hz, 1H), 4.13–4.02 (m, 1H), 3.97–3.84 (m, 1H), 3.72–3.56 (m, 2H), 3.43–3.22 (m, 7H), 3.09–2.79 (m, 4H), 2.51–2.00 (m, 24H), 1.73–1.24 (m, 12H), 1.07 (d, J = 4.8 Hz, 9H), 0.98 (s, 6H) ppm. LC–MS (ESI): *m/z* 1,541.8 $[M+H]^+$.

Preparation of (2S,4R)-1-((S)-2-acetamido-3,3-dimethylbutanoyl)-4-hydroxy-N-((S)-1-(4-(4-methylthiazol-5-yl)phenyl)ethyl)pyrrolidine-2-carboxamide (VHL-L). To a solution of compound 13a (52 mg, 0.108 mmol) and TEA (42 µl, 0.302 mmol) in DCM (5 ml) was added acetic anhydride (10.4 µl, 0.110 mmol). The resulting solution was stirred at room temperature for 1 h. The reaction was quenched with water (5 ml) and extracted with DCM. The organic layer was washed with NH_4Cl solution (aq.) and saline, dried over Na_2SO_4 and concentrated under reduced pressure. The crude product was purified by silica gel flash column chromatography to afford VHL-L (41 mg, yield 78%). ^{1}H NMR (400 MHz, $CDCl_3$) δ 8.69 (s, 1H), 7.47–7.34 (m, 5H), 6.34 (d, J = 8.8 Hz, 1H), 5.17–5.03 (m, 1H), 4.70 (t, J = 7.9 Hz, 1H), 4.61–4.45 (m, 2H), 4.06 (d, J = 11.3 Hz, 1H), 3.70–3.52 (m, 1H), 2.57–2.42 (m, 4H), 2.10–2.03 (m, 1H), 1.98 (s, 3H), 1.48 (d, J = 6.8 Hz, 3H), 1.05 (s, 9H) ppm. LC–MS (ESI): *m/z* 487.2 $[M+H]^+$.

Chemical compounds and antibodies. The information for commercially available chemical compounds, anticancer drugs and antibodies are provided in Supplementary Tables 6 and 7.

Cell lines and cell culture. Human T-ALL MOLT-4 (cat. no. CRL-1582), B-ALL RS4;11 (RS4, cat. no. CRL-1873), SCLC NCI-H146 (H146, cat. no. HTB-173), breast cancer MDA-MB-231 (cat. no. HTB-26), prostate cancer PC-3 (cat. no. CRL-1435), hepatocellular carcinoma HepG2 (cat. no. HB-8065), colorectal carcinoma SW620 (cat. no. CCL-227), renal cell carcinoma 786-O (cat. no. CRL-1932), lung fibroblasts WI-38 (cat. no. CCL-75) and epithelial kidney HEK 293T (293T, cat. no. ACS-4500) cell lines were purchased from American Type Culture Collection (ATCC). Human multiple myeloma cell lines (EJM and NCI-H929 (H929)) were a kind gift from E. Tian at the Winthrop P. Rockefeller Cancer Institute at University of Arkansas for Medical Sciences. MOLT-4, RS4 and H146 cell lines were cultured in RPMI 1640 medium (cat. no. 22400–089, Thermo Fisher Scientific) supplemented with 10% (vol/vol) heat-inactivated fetal bovine serum (FBS, cat. no. S11150H, Atlanta Biologicals, Flowery Branch, GA, USA), 100 U ml^{-1} penicillin and 100 µg ml^{-1} streptomycin (penicillin–streptomycin, cat. no. 15140122, Thermo Fisher Scientific). EJM cells were cultured in RPMI medium with 10% FBS, 100 U ml^{-1} penicillin and 100 µg ml^{-1} streptomycin supplemented with 1% MarrowMAX Bone Marrow Medium (cat. no. 12260014, Thermo Fisher Scientific). H929 cells were cultured in RPMI medium with 10% FBS and 100 U ml^{-1} penicillin and 100 µg ml^{-1} streptomycin supplemented with 0.05 mM 2-mercaptoethanol. All other cell lines were cultured in complete Dulbecco's modified Eagle medium (DMEM, cat. no. 12430054, Thermo Fisher Scientific) with 10% FBS, 100 U ml^{-1} penicillin and 100 µg ml^{-1} streptomycin. All the cell lines were maintained in a humidified incubator at 37 °C and 5% CO_2.

Immunoblotting. Cells were treated with DT2216 and other compounds at indicated concentrations and durations. Untreated and treated cells were harvested and washed once with ice-cold phosphate-buffered saline, pH 7.2 (PBS, cat. no. 20012027; Thermo Fisher Scientific). Adherent cells were harvested using 0.25% Trypsin–EDTA solution (cat. no. 25200056, Thermo Fisher Scientific) and washed with ice-cold PBS. The cell pellets were lysed in radioimmunoprecipitation assay (RIPA) lysis buffer (50 mM Tris-HCl pH 7.4, 150 mM NaCl, 1% NP-40, 0.5% sodium deoxycholate, 0.1% SDS, 5 mM EDTA, 1 mM EGTA; cat. no. BP-115DG, Boston Bio Products, Ashland, MA, USA) supplemented with 1% protease inhibitor cocktail (cat. no. P8340, Sigma-Aldrich, St. Louis, MO, USA) and 1% phosphatase inhibitor cocktail (cat. no. P0044, Sigma-Aldrich). Protein lysates were incubated on ice for 15 min and then kept at −80 °C overnight to allow for complete lysis. The samples were thawed on ice and then centrifuged at maximum speed (14,000 r.p.m.) for 15 min in a refrigerated centrifuge. The protein concentration in the supernatants was determined using the Pierce BCA protein Assay kit (cat. no. 23225, Thermo Fisher Scientific). The protein concentration was normalized and the samples were reduced in 4× Laemmli's SDS-sample buffer (cat. no. BP-110R, Boston Bio Products) and denatured at 95 °C in a heated block. An equal amount of protein samples (20–40 µg per lane) were resolved using precast 4–20% Tris-glycine gels (Mini-PROTEAN TGX, cat. no. 456–1094, Bio-Rad), and resolved proteins were transferred onto 0.2-µm pore size polyvinylidene difluoride (PVDF) blotting membranes (cat. no. LC2002, Thermo Fisher Scientific) using mini trans-blot electrophoretic transfer cell (Bio-Rad). The membranes were blocked with non-fat dry milk (5% wt/vol) in 1× Tris-buffered saline-Tween-20 (TBST, cat. no. J77500, Affymetrix) for 1 h at room temperature, and were subsequently probed with primary antibodies at a predetermined optimal concentration in non-fat dry milk (5% wt/vol in TBST) overnight at 4 °C. The membranes were washed three times (5–10 min each) in TBST and then incubated with horse radish peroxidase (HRP)-conjugated secondary antibodies for 1–1.5 h at room temperature. Following sufficient washing with TBST, the membranes were exposed with chemiluminescent HRP substrate (cat. no. WBKLS0500, MilliporeSigma), and the signal was detected using autoradiography (SRX-101, Konica) or the ChemiDoc MP Imaging System (Bio-Rad). The immunoblots were quantified by densitometry using ImageJ software (NIH) and the data were expressed as relative band intensities normalized to equal loading control.

Viability assays in cancer cells. Cancer cells in complete cell culture medium were seeded in 96-well plates (100 µl per well) at the optimized densities (50,000–100,000 suspension cells, 3,000–5,000 adherent cells). Suspension cells were treated 30 min after seeding, whereas adherent cells were allowed to adhere overnight and were then treated. Compound treatments were prepared in complete cell culture medium and 100 µl of 2× treatment-containing medium were added to each well. Complete cell culture medium without treatment was added in control wells, and wells containing medium without cells served as background. The outer wells of the 96-well plate were not used for treatment and were filled with 200 µl of PBS to reduce evaporation of medium from inner wells. Each compound and/or combination was tested at nine different concentrations with three to six replicates, unless otherwise specified. For combination treatments with DT2216 and ABT199 or DT2216 and S63845, cells were treated with equimolar concentrations in twofold serial dilutions. For combination treatment with DT2216 and chemotherapeutics, cells were treated at equimolar concentrations and threefold serial dilutions, unless otherwise specified. The cell viability was measured after 72 h by tetrazolium-based MTS assay. MTS reagent (2 mg ml^{-1} stock; cat. no. G1111, Promega) was freshly supplemented with phenazine methosulfate (PMS, 0.92 mg ml^{-1} stock, cat. no. P9625, Sigma-Aldrich) in 20:1 ratio, and 20 µl of this mixture was added to each control and treatment well. The cells were incubated for 4 h at 37 °C and 5% CO_2, and then the absorbance was recorded at 490 nm using Biotek's Synergy Neo2 multimode plate reader (Biotek). The average absorbance value of background wells was subtracted from absorbance value of each control and treatment well, and percent cell viability ($(A_t / A_0) \times 100$)) was determined in each treatment well, where A_t is the absorbance value of the treatment well and A_0 is the average absorbance value of control wells after background subtraction. The data were expressed as average percentage cell viability and fitted in non-linear regression curves using GraphPad Prism 7 (GraphPad Software, La Jolla, CA, USA).

Platelet viability assays. Human platelet-rich plasma (PRP) was purchased from Zenbio (cat. no. SER-PRP-SDS). PRP was used for experiments immediately after delivery. PRP was transferred into 50-ml polypropylene tubes, each containing 5 ml acid citrate buffer (cat. no. sc-214744, Santa Cruz Biotechnology). To prevent clotting, prostaglandin E1 (PGE1, cat. no. sc-201223A, Santa Cruz Biotechnology) and apyrase (cat. no. A6237, Sigma-Aldrich) were added to final concentrations of 1 µM and 0.2 units per ml, respectively. After gently mixing the solution, platelets were pelleted by centrifugation at 1,200 *g* for 10 min. Pelleted platelets were gently washed without disruption in 2 ml HEPES-buffered Tyrode's solution

(10 mM HEPES, 135 mM NaCl, 2.8 mM KCl, 1 mM $MgCl_2$, 2 mM $CaCl_2$, 12 mM $NaHCO_3$, 0.4 mM NaH_2PO_4, 0.25% BSA and 5.5 mM glucose, pH 7.4; cat. no. PY-921WB, Boston BioProducts) containing 1 μM PGE1 and 0.2 units ml^{-1} apyrase. After washing, pellets were slowly resuspended in 10 ml HEPES-buffered Tyrode's solution containing 1 μM PGE1 and 0.2 units ml^{-1} apyrase. The number of platelets was counted using a HEMAVET 950FS hematology analyzer (Drew Scientific, Inc.). For viability assays, platelet number was adjusted to 2×10^8 per ml in HEPES-buffered Tyrode's solution containing 1 μM PGE1, 0.2 units ml^{-1} apyrase and 10% FBS. Each treatment was given in 2 ml platelet suspension in 15-ml polypropylene tubes for 72 h. The tubes were placed on a rotating platform at room temperature for the duration of treatment. After 72 h treatment, 200 μl of untreated or treated platelets were plated in each well of 96-well plates, and the viability was measured by MTS assay as described in the previous method.

Determination of EC_{50} and combination index. Dose–response curves (Variable slope, four parameters) were generated for each test compound, and their EC_{50} values were determined using GraphPad Prism 7. The combination indices (CIs) were determined using Compusyn version 1.0 software (http://www.combosyn.com). CI < 0.3 was considered to be a strong synergistic effect induced by two compounds when they were used in combination. The average of CI at EC_{75} (concentration with 75% loss of cell viability) and EC_{90} (concentration with 90% loss of cell viability) are presented in Fig. 5 and Supplementary Table 5 as a more accurate measure of synergy by different combinations.

Caspase-3 activity assay. The caspase-3 activity in untreated and treated cells was measured using EnzChek caspase-3 assay kit no. 2, Z-DEVD-R110 substrate (cat. no. E13184, Thermo Fisher Scientific) following manufactures' instructions. Briefly, MOLT-4 cells were seeded in 60-mm dishes (2.5×10^6 cells in 5 ml complete cell culture medium per dish), and then treated with indicated concentrations of DT2216 or ABT263 for 24 h. Cells were lysed in 1× cell lysis buffer by subjecting them to a freeze–thaw cycle in ice-ethanol bath or by 30-min incubation on ice. After centrifugation at 5,000 r.p.m. for 5 min, 50 μl of supernatant from each sample was transferred into duplicate microplate wells, and 50 μl of 2× substrate solution was added to each well. 50 μl of lysis buffer and 50 μl of 2× substrate solution was added to background wells. After incubation for 30 min at room temperature, fluorescence was measured (excitation/emission ~ 496/520 nm) using a Biotek's Synergy Neo2 multi-mode plate reader. The data were expressed as percent caspase-3 activity ($((F_t / F_0) \times 100)$), where F_t is the fluorescence value of the treatment well and F_0 is the average fluorescence value of control wells after background subtraction.

***BAK* (*BAK1*) and *BAX* double-knockout by CRISPR–Cas9 genomic editing.** To deplete BAK and BAX, the sgRNAs targeting human *BAK* and *BAX* were designed and cloned into lentiCRISPR v2 vector (a gift from F. Zhang; Addgene plasmid no. 52961). Packaging 293T cells were transfected with *BAK* and *BAX* sgRNAs or negative control (non-targeting sgRNA-sgCTRL)[59] and helper vectors (pMD2.G and psPAX2; Addgene nos. 12259 and 12260) using lipofectamine 2000 reagent (cat. no. 11668019, Life Technologies). Medium containing lentiviral particles and 8 μg ml^{-1} polybrene (Sigma-Aldrich) was used to infect H146 cells. Infected cells were selected in medium containing 1 μg ml^{-1} puromycin. The target guide sequences are as follows: *BAK*-sg1, forward (5′-CACCGTCATCGGGGACGACATCAAC-3′) and reverse (5′-AAACGTTGATGTCGTCCCCGATGAC-3′); *BAK*-sg2, forward (5′-CACCGCTGCAACCTAGCAGGTGAGC-3′) and reverse (5′- AAACGCTCACCTGCTAGGTTGCAGC-3′); *BAX*-sg1, forward (5′-CACCGGGATCGAGCAGGGCGAATGG-3′) and reverse (5′-AAACCCATTCGCCCTGCTCGATCCC-3′); *BAX*-sg2: forward (5′-CACCGAGCGAGTGTCTCAAGCGCAT-3′) and reverse (5′-AAACATGCGCTTGAGACACTCGCTC-3′).

Immunoprecipitation. Human cancer cells or platelets were lysed in Pierce IP lysis buffer (25 mM Tris-HCl pH 7.4, 150 mM NaCl, 1 mM EDTA, 1% NP-40 and 5% glycerol; cat. no. 87787; Thermo Fisher Scientific) supplemented with 1% (vol/vol) protease and phosphatase inhibitor cocktail (cat. no. PPC1010; Sigma-Aldrich). Lysates were precleared by incubating with 1 μg of mouse IgG (cat. no. sc-2025; Santa Cruz Biotechnology) and 20 μl of protein A/G-PLUS agarose beads (25% vol/vol; cat. no. sc-2003; Santa Cruz Biotechnology) for 30 min at 4 °C. 1,000 μg of cell lysates were incubated with 2 μg of anti-BCL-X_L (cat. no. sc-56021; Santa Cruz Biotechnology) or anti-IgG for 1 h followed by addition of 25 μl of protein A/G-PLUS agarose beads and incubated overnight at 4 °C. Immunoprecipitates were collected by centrifugation and washed 2–3 times with IP lysis buffer. Samples were mixed with Laemmli's SDS-buffer, denatured and analyzed by SDS–polyacrylamide gel electrophoresis (SDS–PAGE) and immunoblotting. An anti-rabbit HRP-conjugated Fc-fragment-specific secondary antibody directed against primary antibodies was used to detect immune complexes in immunoblotting.

AlphaScreen for the determination of DT2216-BCL-X_L, BCL-2 and BCL-W binding affinity. To evaluate the binding affinities of DT2216 and ABT263 towards BCL-X_L, BCL-2 and BCL-W, AlphaScreen competitive binding assays were performed. The assays were performed at room temperature and reagents were diluted in a buffer containing 250 mM HEPES pH 7.5, 1 M NaCl, 1% BSA and 0.05% Tween-20. Purified recombinant histidine (His)-tagged BCL-X_L (0.1 nM, cat. no. SRP0187, Sigma-Aldrich), BCL-2 (0.2 nM, cat. no. SRP0186, Sigma-Aldrich) or BCL-W (0.2 nM, cat. no. B1059, Sigma-Aldrich) were incubated with increasing concentrations of DT2216 or ABT263 and 15 nM biotin-tagged BAD (biotin-LWAAQRYGRELRRMSDEFEGSFKGL amino-terminal, AnaSpec) or 30 nM BIM peptides (biotin-MRPEIWIAQELRRIGDEFNA N-terminal, AnaSpec) to a final volume of 40 μl in 96-well PCR plate. BAD peptide was used to assess the binding affinity of compounds towards BCL-X_L, whereas BIM peptide was used for BCL-2 and BCL-W. After 24 h incubation, 5 μl 6× His-acceptor beads (cat. no. AL128M, PerkinElmer) were added to each well at 20 μg ml^{-1} final concentration and incubated for 1 h. Thereafter, 5 μl streptavidin-donor beads were added (cat. no. 6760002, PerkinElmer) to each well at 20 μg ml^{-1} final concentration and incubated for 30 min. At the end of the incubation period, 17 μl of each sample was transferred in adjacent wells of 384-well proxy plate (cat. no. 6008280, PerkinElmer). The plate was scanned using the Alpha program on Biotek's Synergy Neo2 multimode plate reader. The inhibition constant (K_i) was calculated using the non-linear regression, one site, competitive binding, Fit K_i function on GraphPad Prism 7 software, based on experimentally determined dissociation constant (K_D) for each protein–peptide pair.

Proteomics analysis. *Sample preparation and LC–MS/MS analysis.* To label cells with stable isotopic amino acids (SILAC), WI-38 cells were propagated in DMEM SILAC medium deficient in both L-lysine and L-arginine (cat. no. 88364, Thermo Fisher Scientific) and supplemented with light-labeled lysine ($[^{12}C_6{}^{14}N_2]$Lys) and arginine ($[^{12}C_6{}^{14}N_4]$Arg) for light state (cat. no. 89987 and no. 89989; Thermo Fisher Scientific), and $[^{13}C_6{}^{15}N_2]$Lys and $[^{13}C_6{}^{15}N_4]$Arg for heavy-state labeling (cat. no. 88209 and no. 89990, Thermo Fisher Scientific). Cells were cultured for at least six doubling times for complete incorporation. The light-labeled WI-38 cells were untreated (DMSO), and the heavy-labeled WI-38 cells were treated with 1 μM DT2216 or DT2216NC for 6 h, respectively. Reverse labeling was used in the second biological replicate. The untreated and DT2216- or DT2216NC-treated cells were collected by centrifugation at 500*g* for 5 min. Pellets were washed twice by resuspension in 1 ml of ice-cold PBS. The cell pellets were resuspended in 20 ml freshly prepared lysis buffer (2% SDS, 100 mM Tris/HCl pH 7.6) containing MS-SAFE Protease and Phosphatase Inhibitor (cat. no. MSSAFE-5VL, Sigma-Aldrich) for sonication. The lysate was centrifuged at 15,000*g* for 10 min at 18 °C. The supernatant was stored at −80 °C for proteomics analysis. Protein concentration was measured by BCA assay (cat. no. 23227, Thermo Fisher Scientific), and SILAC pairs were mixed in equimolar amounts. Purified proteins were reduced, alkylated and digested using filter-aided sample preparation[60]. Tryptic peptides were separated into 36 fractions on a 100 × 1.0 mm Acquity BEH C18 column (cat. no. 186002350, Waters) using an UltiMate 3000 UHPLC system (Thermo Fisher Scientific) with a 40-min gradient from 99:1 to 60:40 buffer A (0.1% formic acid, 0.5% acetonitrile):B (0.1% formic acid, 99.9% acetonitrile) ratio under basic pH conditions, and then consolidated into 12 super-fractions. Each super-fraction was then further separated by reverse phase XSelect CSH C18 2.5-μm resin (cat. no. 186006109, Waters) on an in-line 150 × 0.075 mm column using an UltiMate 3000 RSLCnano system (Thermo Fisher Scientific). Peptides were eluted using a 60-min gradient from 97:3 to 60:40 buffer A:B ratio. Eluted peptides were ionized by electrospray (2.15 kV) followed by MS/MS analysis using higher-energy collisional dissociation (HCD) on an Orbitrap Fusion Lumos mass spectrometer (Thermo Fisher Scientific) in top-speed data-dependent mode. MS data were acquired using the FTMS analyzer in profile mode at a resolution of 240,000 over a range of 375 to 1,500 *m/z*. Following HCD activation, MS/MS data were acquired using the ion trap analyzer in centroid mode and normal mass range with precursor mass-dependent normalized collision energy between 28.0 and 31.0.

Raw data processing. Proteins were identified and SILAC ratios determined using MaxQuant with a parent ion tolerance of 3 ppm and a fragment ion tolerance of 0.5 Da. The derived peak list was searched with the built-in Andromeda search engine against the reference human proteome downloaded from Uniprot (http://www.uniprot.org/) on 13 March 2018. The search parameters for both algorithms included carbamidomethylation of cysteine residues as a fixed modification and N-terminal acetylation, oxidation at methionine, and SILAC labeling $[^{13}C_6{}^{15}N_2]$Lys and $[^{13}C_6{}^{15}N_4]$Arg as variable modifications. Trypsin was specified as the protease, and a maximum of two missed cleavages were allowed. The data were screened against a target decoy database and the false discovery rate (FDR) was set to 1% at the peptide level and contained at least 2 identified peptides. Protein probabilities were assigned by the Protein Prophet algorithm[61]. Statistical analysis was performed using Perseus software[62]. A threshold with SILAC ratio greater than 1.5-fold and *q* value of 0.05 for the Benjamini–Hochberg false-discovery rate were used to identify the proteins with significant changes. The MS data have been deposited to the ProteomeXchange Consortium (http://proteomecentral.proteomexchange.org) through the PRIDE partner repository[63] with the dataset identifier PXD010878.

Cellular thermal shift assay. The cellular thermal shift assay (CETSA) was adapted from Smith et al.[48]. Briefly, 2.5×10^7 MOLT-4 or RS4 cells were treated

with 1 μM DT2216 or DMSO for 6 h, and then were collected, washed with PBS and resuspended in PBS containing protease and phosphatase inhibitors. For MOLT-4 cells, 10 μM MG132 was added in to prevent the degradation of BCL-X_L. The resuspended cells were freeze–thawed four times with liquid nitrogen. After each freeze–thaw cycle, lysate was vortexed briefly to ensure homogenous thawing. The soluble fraction was separated from cell debris by centrifugation at 20,000*g* for 30 min at 4 °C and then heated at gradient temperature from 42 °C to 69.5 °C for 3 min and cooled down to 25 °C for another 3 min. The treated samples were centrifuged at 20,000*g* for 30 min at 4 °C to remove the denatured proteins and then were analyzed by immunoblotting.

AlphaLISA assay for ternary complex formation. We used AlphaLISA assay to monitor ternary complex formation between target protein, PROTAC and E3 ligase, as described previously[44,58]. To validate the formation of the ternary complex of BCL-X_L or BCL-2, DT2216 and the VHL E3 ligase, a fixed concentration of His-tagged recombinant proteins (100 nM BCL-X_L and 10 nM BCL-2) and recombinant active glutathione-*S*-transferase (GST)-tagged VHL–elongin B–elongin C–Cul2 complex (50 nM for BCL-X_L, 5 nM for BCL-2; cat. no. 029641, US Biological) was incubated with varying concentrations of test compounds in fourfold serial dilutions, to a final volume of 40 μl in a 96-well PCR plate. After 30 min of incubation at room temperature, 5 μl alpha glutathione-donor beads (cat. no. 6765300, PerkinElmer) were added to each well to 20 μg ml^{-1} final concentration and incubated for 15 min. Thereafter, 5 μL 6× His-acceptor beads were added to each well at 20 μg ml^{-1} final concentration and incubated for an additional 45 min at room temperature. Thereafter, 17 μl of each sample was transferred in adjacent wells of 384-well proxy plate, and the plate was scanned using the Alpha program on Biotek's Synergy Neo2 multimode plate reader. The data were expressed as average AlphaLISA signal and plotted against different concentrations of compounds.

nanoBRET ternary complex formation assay. Plasmids were purified on miniprep columns according to the manufacturer's protocol (cat. no. 27106 Qiagen). Plasmids HaloTag-VHL (cat. no. CS1679C155) and CMV LgBit (cat. no. CS1956B03) were purchased from Promega. HiBit-BCL-X_L (pDL2288) and HiBit-BCL-2 (pDL2306) were constructed based on pBiT3.1 N-HiBiT (cat. no. N2361, Promega), pLX304-BCL-X_L (DNASU plasmid cat. no. HsCD00437924) and Flag-BCL-2 (a gift from C. Distelhorst, Addgene plasmid no.18003) plasmids through Gibson assembly method (Gibson Assembly Master Mix, cat. no. E2611S, NEB) using the primers as follows. pBiT3.1-N-BCL-X_L-FP1: 5′-TGGCTCGAGC-GGTGGGAATTCTGGTATGTCTCAGAGCAACCGGGAGCTGGTG-3′; pBiT3.1-N-BCL-X_L-RP1: 5′-TCTTCCGCTAGCTCCACCGGATCCTCCTCATT TCCGACTGAAGAGTGAGCC-3′; pBiT3.1-N-BCL-X_L-Vector-FP1: 5′-GGCTC-ACTCTTCAGTCGGAAATGAGGAGGATCCGGTGGAGCTAGCGGAAGA-3′; pBiT3.1-N-BCL-X_L-Vector-RP1: 5′-CACCAGCTCCCGGTTGCTCTGAGACATA-CCAGAATTCCCACCGCTCGAGCCA-3′; pBiT3.1-N-BCL-2-FP1: 5′-TGGCTC-GAGCGGTGGGAATTCTGGTATGGCGCACGCTGGGAGAACAGGGTAC-3′; pBiT3.1-N-BCL-2-RP1: 5′-TCTTCCGCTAGCTCCACCGGATCCTCCTCACT TGTGGCCCAGATAGGCACCCAG-3′; pBiT3.1-N-BCL-2-Vector-FP1: 5′-CTG GGTGCCTATCTGGGCCACAAGTGAGGAGGATCCGGTGGAGCTAGCGG AAGA-3′; pBiT3.1-N-BCL-2-Vector-RP1: 5′-GTACCCTGTTCTCCCAGCGTG CGCCATACCAGAATTCCCACCGCTCGAGCCA-3′. DNA sequences in these plasmids were authenticated by automatic sequencing. 293T cells (8×10^5) were transfected with Lipofectamine 2000 reagent (cat. no. 11668019, Thermo Fisher Scientific) and 1 μg HaloTag-VHL, 10 ng HiBit-BCL-X_L and 10 ng LgBit or 1 μg HaloTag-VHL, 10 ng HiBit-BCL-2 and 10 ng LgBit. After 24 h, 2×10^4 transfected cells were seeded into white 96-well tissue culture plates in FluoroBrite DMEM (cat. no. A18967-02, Thermo Fisher Scientific) containing 4% FBS with or without HaloTag NanoBRET 618 Ligand (cat. no. PRN1662, Promega) and incubated overnight at 37 °C, 5% CO_2. The following day, different doses of DT2216 were added into the medium, and plates were incubated at 37 °C, 5% CO_2, for 6 h. After treatment, NanoBRET Nano-Glo Substrate (cat. no. N1662, Promega) was added into the medium, and the contents were mixed by shaking the plate for 30 s before measuring donor and acceptor signals on Biotek plate reader. Dual-filtered luminescence was collected with a 450/50 nm bandpass filter (donor, NanoBiT-BCL-X_L protein or NanoBiT-BCL-2 protein) and a 610-nm longpass filter (acceptor, HaloTag NanoBRET ligand) using an integration time of 0.5 s. mBRET ratios were calculated following the NanoBRET Nano-Glo Detection System (cat. no. N1662, Promega).

Coimmunoprecipitation assay for the determination of BCL-X_L and BCL-2 ubiquitination. Plasmid pSG5-Flag-BCL-X_L (pDL2009) was constructed based on pSG5-Flag vector (a gift from D. Hayward at Johns Hopkins University, which was originally generated by Stratagene) and pLX304-BCL-X_L (DNASU plasmid cat. no. HsCD00437924) through the Gibson assembly method. The following two primers sets were used: primer set-1, forward (5′-GACTACAAGGACGACGATGACAAGGGATCT ATGTCTCAGAGCAACCGGGAGCTGGTG-3′) and reverse (5′-GTTCTGCTTT AATAAGATCTGGATCTTCATTTCCGACTGAAGAGTGAGCCCAGCAGA AC-3′); primer set-2, forward (5′-GTTCTGCTGGGCTCACTCTTCAGT-CGGAAATGAAGATCCAGATCTTATTAAAGCAGAAC-3′) and reverse (5′-CACCAGCTCCCGGTTGCTCTGAGACATAGATCCCTTGTCA-TCGTCGTCCTTGTAGTC-3′). The DNA sequence of the plasmid was authenticated by automatic sequencing. 293T cells were cotransfected with Flag-BCL-X_L and HA-tagged ubiquitin (a gift from T. Dawson, Addgene, Plasmid no. 17608) or Flag-BCL-2 (a gift from C. Distelhorst, Addgene plasmid no. 18003) and HA-ubiquitin for 40 h, and then were treated with DMSO or 1 μM DT2216 for 4 h, and 10 μM MG132 was added to prevent protein degradation. Proteins were extracted by using immunoprecipitation lysis buffer (cat. no. 87788, Thermal Fisher Scientific) and then subjected to immunoprecipitation using Anti-FLAG M2 Magnetic Beads (cat. no. M8823, Sigma-Aldrich) according to the manufacturer's protocol. Anti-FLAG M2 Magnetic Beads was washed with 1× TBS three times and then added to protein samples, and the mixture was incubated at 4 °C with rotation overnight. The magnetic beads were collected and then washed three times with 1× TBS. Immunoprecipitated samples were eluted with 2× SDS sample buffer and boiled 5 min at 95 °C.

Mutational analysis. Flag-BCL-X_L-K87R, Flag-BCL-X_L-K87H, Flag-BCL-X_L-K157R, Flag-BCL-X_L-K-ko, and Flag-BCL-X_L-K87-only were constructed based on pSG5-Flag-BCL-X_L (pDL2009) (mentioned above) using QuikChange II site-directed mutagenesis kit (Agilent Technologies) and the following primer sets: BCL-X_L-K87R forward (5′-GTGATCCCCAT-GGCAGCAGTAAGGCAAGCGCTGAGGGAGGCAGGC-3′) and reverse (5′-GCCTGCCTCCCTCAGCGCTTGCCTTACTGCTGCCATGGGGATCAC-3′); BCL-X_L-K87H forward (5′-CCCATGGCAGCAGTACATCAAGCGCTGAGG GAG-3′) and reverse (5′-CTCCCTCAGCGCTTGATGTACTGCTGCCATGG G-3′); BCL-X_L-K157R forward (5′-TGTGCGTGGAAAGCGTAGACAGGGA GATGCAGG-3′) and reverse (5′-CCTGCATCTCCCTGTCTACGCTTTCCA CGCACA-3′). BCL-X_L-K-ko was constructed by mutating each of the six Lys residues (Lys 16, Lys 20, Lys 87, Lys 157, Lys 205, and Lys 233) to Arg by the primers mentioned above and the following primer sets: BCL-X_L-K16R and -K20R forward (5′-GTGGTTGACTTTCTCTCCTACAGGCTTTCCCAGA GAGGATACAGCTGGAGTCAGT-3′) and reverse (5′-ACTGACTCCAG CTGTATCCTCTCTGGGAAAGCCTGTAGGAGAGAAAGTCAACCAC-3′); BCL-X_L-K205R forward (5′-CAATGCAGCAGCCGAGAGCCGAAGGGGCC-AGGAACGCTTCAACCGC-3′) and reverse (5′-GCGGTTGAAGCGTTCCT GGCCCCTTCGGCTCTCGGCTGCTGCATTG-3′); BCL-X_L-K233R forward (5′-CTGGGCTCACTCTTCAGTCGGAGATGAAGATCCAGATCTTATTAA-3′) and reverse (5′-TTAATAAGATCTGGATCTTCATcTCCGACTGAAGAGT GAGCCCAG-3′). BCL-X_L-K87-only was constructed by mutating each of the five Lys residues (Lys 16, Lys 20, Lys 157, Lys 205 and Lys 233), excluding Lys 87, to Arg by the primers mentioned above. DNA sequences in all these plasmids were authenticated by automatic sequencing.

Identification of ubiquitination site in BCL-X_L. *Enrichment of Flag-tagged protein for mass spectrometry.* 293T cells were cotransfected with Flag-BCL-X_L (pDL2009) and HA-ubiquitin vectors, or Flag-BCL-2 and HA-ubiquitin vectors. Proteins were extracted by immunoprecipitation lysis buffer and then subjected to immunoprecipitation using Pierce Anti-DYKDDDDK Affinity Resin (cat. no. A36801, Thermal Fisher Scientific) according to the manufacturer's protocol. Anti-DYKDDDDK Affinity Resin was washed with 1× TBS three times and then added to protein samples, and the mixture was incubated at 4 °C with rotation for 4 h. The immunoprecipitated samples were centrifuged at 1,000*g* for 1 min at 4 °C, and then washed three times with 1× TBS. Immunoprecipitated samples were eluted with 0.1 M glycine HCl (pH 2.8).

Sample preparation and LC–MS/MS. Purified proteins were reduced, alkylated and digested using filter-aided sample preparation[60]. Resulting peptides were then separated by reverse phase XSelect CSH C18 2.5-μm resin (Waters) on an in-line 150 × 0.075 mm column using an UltiMate 3000 RSLCnano system (Thermo Fisher Scientific). Peptides were eluted using a 90-min gradient from 97:3 to 60:40 buffer A:B ratio A (buffer A: 0.1% formic acid and 0.5% acetonitrile in water, buffer B: 0.1% formic acid in acetonitrile). Eluted peptides were ionized by electrospray (2.15 kV), followed by MS/MS analysis using higher-energy collisional dissociation (HCD) on an Orbitrap Fusion Lumos mass spectrometer (Thermo Fisher Scientific) in top-speed data-dependent mode. MS data were acquired using the FTMS analyzer in profile mode at a resolution of 240,000 over a range of 375 to 1,500 *m/z*. Following HCD activation, MS/MS data were acquired using the ion trap analyzer in centroid mode and the normal mass range with precursor-mass-dependent normalized collision energy between 28 and 31.

Proteomics data analysis. Proteins were identified by a database search against the human Uniprot database (73,911 proteins, 16 March 2019) using Mascot with a parent ion tolerance of 3 ppm and a fragment ion tolerance of 0.5 Da. Methionine oxidation (+15.99492 Da), protein N-terminal acetylation (+42.03670) and lysine ubiquitination (+114.04293 Da) were variable modifications; cysteine was assigned a fixed carbamidomethyl modification (+57.021465 Da). Percolator was used to filter the peptide spectrum matches to a false-discovery rate of 1%. Scaffold (Proteome Software) was used to verify MS/MS-based peptide and protein

identifications. Protein identifications were accepted if they could be established with a false-discovery rate that was <1% and contained at least 2 identified peptides. Protein probabilities were assigned by the Protein Prophet algorithm[61]. The MS data have been deposited to the ProteomeXchange Consortium (http://proteomecentral.proteomexchange.org) through the PRIDE partner repository[61] with the dataset identifier PXD015454.

Mice. Female CB17/Icr-*Prkdc*^{scid}/IcrIcoCrl (CB-17 SCID), CB17.Cg-*Prkdc*^{scid}*Lyst*$^{bg-J}$/Crl (CB-17 SCID-beige) or NOD.CB17-Prkdc^{scid}/NCrCrl (NOD-SCID) mice aged 5–6 weeks were purchased from Charles River Laboratories, and were housed in the Assessment and Accreditation of Laboratory Animal Care (AAALAC)-accredited animal facilities at University of Arkansas for Medical Sciences (UAMS) or University of Florida (UF) under pathogen-free conditions. Female NOD-SCID IL2Rgnull (NSG) mice aged 6–7 weeks were purchased from Jackson Laboratory (Bar Harbor, Main, USA) and were housed in the AAALAC-accredited animal facilities at MD Anderson Cancer Center (MDACC) under pathogen-free conditions. Mice received food and water ad libitum and were allowed to acclimate for 1–2 weeks before being used for experiments at the age of 6–8 weeks. All animal work was approved and done in accordance with the approvals from the Institutional Animal Care and Use Committees of UAMS, UF and MDACC with the exception of the pharmacokinetic (PK) studies that were done by BioDuro, a global contract research organization, through a contract. All animal studies complied with the ethical regulations and humane endpoint criteria according to the NIH Guidelines for the Care and Use of Laboratory Animals.

Analysis of DT2216 in tumor samples. A bioanalytical method was developed for the quantification of DT2216 in tumor homogenates using a Waters Xevo TQ-S Micro triple quadrupole mass spectrometer and Acquity Class I UPLC. Chromatographic separation was achieved using a mobile phase consisting of aqueous ammonium acetate buffer (10 mM, pH 3.5) (pump A) and acetonitrile (pump B) on a Waters Acquity BEH C18 column (1.7 µm, 2.1 × 50 mm). A gradient method started with pump B supplying 15% of acetonitrile up to 0.5 min. The composition of acetonitrile was linearly increased to 80% until 1.5 min and kept constant until 3.0 min. The composition of acetonitrile was immediately decreased to 15% at 3.0 min and kept constant until 3.5 min. The flow rate of the mobile phase was 0.35 ml min^{-1} and the injection volume was 2 µl. Analysis of DT2216 was performed using ESI in the positive mode. Capillary voltage, cone gas, desolvation gas, desolvation temperature and source temperature were optimized for maximum analyte response and held at 3.0 kV, 50 L per h (flow rate), 900 L per h (flow rate), 450 °C and 150 °C, respectively. The mass spectral analysis of DT2216 and the internal standard (amiodarone) was achieved by multiple-reaction monitoring (MRM). Compound parameters are detailed in Supplementary Table 8. Data acquisition and quantitation were performed using MassLynx and TargetLynx XS software version 4.2. For the bioanalysis of DT2216, pieces of tumor samples were weighted and homogenized in water (1:4, %wt/vol) using a tissue homogenizer (Dremel, BioSpec Products). Sample cleanup (20 µl) was performed by a protein-precipitation method using acetonitrile containing the internal standard (40 ng ml^{-1}) as a quenching solution (80 µl). Calibration (5, 10, 50, 100, 200, 400 and 500 ng ml^{-1}) and quality-control standards (5, 7.5, 250 and 450 ng ml^{-1}) were prepared in drug-free tumor homogenate and analyzed using the ultra-performance LC–MS/MS method. The method was linear for a calibration range of 5–500 ng ml^{-1}. The accuracy and precision calculated for the method were within the specified limits[64] Test samples were analyzed along with freshly prepared calibration and quality-control standards (Extended Data Fig. 5d). Tumor concentration-time data were subjected to non-compartmental analysis, and pharmacokinetic parameters were calculated using Phoenix WinNonlin, version 6.1.

Pharmacodynamics of BCL-X$_L$ degradation by DT2216. MOLT-4 xenografts were established in female CB-17 SCID-beige mice as described in following methods. Tumor-bearing mice were treated with single injection of vehicle or DT2216 (15 mg per kg body weight, i.p.) when the tumors were ~600 mm^3 in size. Two mice each from vehicle- and DT2216-treated groups were euthanized at each time point as indicated in the figure legend of Fig. 4b, and tumors were collected. The proteins were extracted from tumors and used for BCL-X$_L$ degradation by immunoblot analysis. Some portion of these tumors was used for DT2216 analysis as described in the previous method.

Protein extraction from tumors for immunoblotting. Following resection, the tumors were snap frozen and stored at −80 °C until later use. Tumor tissue (~50 mg wet tissue) was lysed in 1 ml of RIPA lysis buffer supplemented with 1% protease inhibitor cocktail and 1% phosphatase inhibitor cocktail. The tissues were kept on ice and were homogenized with the help of a hand homogenizer. The samples were incubated on ice for 2–3 h and then kept at −80 °C overnight to allow for complete lysis. The subsequent sample preparation and immunoblotting were performed as described in the immunoblotting method.

In vivo platelet toxicity assays. *Single dosing with DT2216 or ABT263.* Female 5–6 weeks old CB-17 SCID-beige mice were treated with single i.p. doses of DT2216 (7.5, 15 and 25 mg per kg body weight) or single p.o. doses of ABT263 (25, 50 and 100 mg per kg body weight). Approximately 50 µl of blood was collected at different time points from each mouse as described in the Fig. 4c legend via submandibular plexus route in EDTA tubes (RAM Scientific), and platelets were enumerated using an automated hematology analyzer HEMAVET 950FS (Drew Scientific).

Daily dosing with ABT263 or once a week with DT2216. Female CB-17 SCID-beige mice were treated with ABT263 (50 mg per kg body weight per day, p.o.) or DT2216 (15 mg per kg body weight per week, i.p.). Approximately 50 µl of blood was collected from each mouse 6 h (0.25 d) after each dose of ABT263 or collected from each mouse after 0.25 d, 1.25 d, 2.25 d, 3.25d, 4.25 d, 5.25 d, 6.25 d, 7.25 d, 8.25 d, 9.25 d, 10.25 d, 11.25 d, 12.25 d, 17.25 d and 24.25 d of once per week dosing with DT2216. Platelets were enumerated using HEMAVET 950FS.

Complete blood-cell counts. Approximately 50 µl of blood was collected from each mouse in EDTA tubes via submandibular plexus or retro-orbital bleeding. The mice were anaesthetized with isoflurane inhalation for retro-orbital bleeding. The blood was immediately used for complete blood counts (CBCs) using an automated hematology analyzer HEMAVET 950FS. The data were expressed as number of different blood cells or platelets per µl of blood.

MOLT-4 T-ALL xenograft mouse model. To test the effect of DT2216 on tumor growth in MOLT-4 T-ALL xenografts, MOLT-4 T-ALL cells were collected and suspended in regular RPMI medium and mixed with Matrigel (1:1) (cat. no. 356231, Corning). The cells (5×10^6 cells) suspended in 100 µL of RPMI medium–matrigel mixture were subcutaneously (s.c.) implanted in the right flank of CB-17 SCID mice. Tumor growth was monitored daily, and tumors were measured twice per week using Vernier caliper or digital calipers. Tumor volume was determined using the formula $((L \times W^2) \times 0.5)$, where L is length in mm and W is the width in mm. The treatment started once the average tumor volume reached 150–200 mm^3. The animals were randomly assigned into separate groups ($n = 6$–8 animals per group) such that each group had nearly equal starting average tumor volume. Mice were weighed twice a week, and the treatments were given according to average mouse weight within each group before initiation of treatment. DT2216 and ABT263 for i.p. administration were formulated in 50% phosal 50 PG, 45% miglyol 810 N and 5% polysorbate 80. DT2216 and ABT263 were administered via i.p. injection at 15 mg per kg body weight per week in 100 µl vehicle (Extended Data Fig. 8). ABT263 for oral administration was formulated in 10% ethanol, 30% polyethylene glycol (PEG) 400 and 60% phosal 50 PG (Fig. 4). Control mice received 100 µl vehicle via i.p. injection. A mouse was euthanized when its maximum tumor size reached the humane endpoint, defined according to institutional policy concerning tumor endpoints in rodents. In addition, to prevent excessive pain or distress, the mice were euthanized if the tumors became ulcerated or if the mice showed any signs of ill health. Mice were euthanized by CO_2 suffocation followed by cervical dislocation, and then various tissues including tumors were collected for further analyses.

H146 small-cell lung cancer xenograft model. To test the effect of DT2216 alone or in combination with ABT199 on tumor growth in H146 SCLC xenografts, 5×10^6 H146 SCLC cells were suspended in regular RPMI medium, mixed with Matrigel, and s.c. implanted in the right flank of female CB-17 SCID mice as described in the previous method. Tumor growth was monitored, tumors were measured and the tumor volume was determined as mentioned in the previous method. The treatment started after 4 weeks of cell implantation as shown in Fig. 5c. The animals were randomly assigned into groups treated with vehicle, DT2216 15 mg per kg body weight per week (i.p. injection), ABT263 15 mg per kg body weight per week (i.p. injection), ABT199 50 mg per kg body weight per day (p.o.), and DT2216 + ABT199. DT2216 and ABT263 were formulated as described above. ABT199 was formulated for oral dosing in 60% phosal 50 PG, 30% PEG 400 and 10% ethanol. All the animals were euthanized in accordance with institutional policy, and various tissues were collected. Tumors were weighed and used for BCL-X$_L$, BCL-2 and MCL-1 expression by immunoblotting.

MDA-MB-231 BC xenograft model. To test the effect of DT2216 in combination with docetaxel on tumor growth in MDA-MB-231 breast cancer xenografts, 5×10^6 MDA-MB-231 cells were suspended in regular RPMI medium, mixed with matrigel, and s.c. implanted in the right flank of female NOD-SCID mice. The animals were randomly assigned to vehicle, DT2216 (15 mg per kg body weight, q4d, i.p.), docetaxel (7.5 mg per kg body weight, q14d, i.v.) and DT2216 + docetaxel groups when the average tumor volume reached ~130 mm^3. Docetaxel was dissolved in 5% DMSO + 30% PEG 300 + 5% Tween 80 + 60% distilled H_2O. The solution was filter sterilized to obtain clear solution for intravenous administration. DT2216 was administered 2 d before starting dosing with docetaxel, as also mentioned in Fig. 6c.

T-ALL patient-derived xenograft models. CUL76 and 332×-Luci T-ALL PDX models were kind gifts from A. Ferrando (Columbia University, New York, NY, USA) and K. Yong-Mi (Children's Hospital Los Angeles, Los Angeles, CA), respectively. The D115 T-ALL PDX model was from M. Konopleva's Lab (UTMDACC, Houston, TX). The use of these models was in accord with the Declaration of Helsinki using

an Institutional Review Board (IRB)-approved protocol from MDACC. To establish T-ALL PDX mouse models, 8-week-old NSG mice were sublethally irradiated (0.25 Gy) 24 h prior to cell inoculation. PDX cells (1×10^6) were suspended in PBS and injected into mice through the tail vein. Tumor engraftment was determined by costaining with human and murine anti-CD45 (BioLegend, San Diego, CA) in bone-marrow aspiration samples (CUL76 and D115 T-ALL) or in peripheral blood (332X-Luci) at 10 d post injection. Mice were randomized into different groups. CUL76 PDX were treated with DT2216 (15 mg per kg body weight, q4d, i.p.), ABT199 (100 mg per kg body weight, qd, p.o.), chemotherapy (vincristine 0.15 mg per kg body weight + dexamethasone 5 mg per kg body weight + L-asparaginase 1,000 Units per kg body weight, i.p., weekly), a combination of DT2216 and ABT199 or chemotherapy or ABT199 plus chemotherapy as shown in Fig. 6f. D115 and 332X-Luci PDXs were treated with DT2216, chemotherapy or a combination of DT2216 and chemotherapy as shown in Extended Data Fig. 10. Mice were monitored for disease progression by weekly assessment of leukemic ($hCD45^+$) cells in the peripheral-blood or bone-marrow aspirates and followed for survival.

Statistical analyses. All the graphs presented in this manuscript were made and statistical analyses were performed using GraphPad Prism 7 software. For analysis of means of three or more groups, analysis of variance (ANOVA) tests were performed. In the event that ANOVA justified post hoc comparisons between group means, the comparisons were conducted using Tukey's multiple-comparisons test. Two-sided unpaired Student's *t*-test was used for comparisons between the means of two groups. A Kaplan–Meier test was used for the survival rate in Fig. 6h and Extended Data Fig. 10b,d, and the data were statistically analyzed using log-rank (Mantel–Cox) test. $P < 0.05$ was considered to be statistically significant. The precise *P* values have been provided wherever possible and appropriate.

Reporting Summary. Further information on research design is available in the Nature Research Reporting Summary linked to this article.

Data availability

The MS data have been deposited to the ProteomeXchange Consortium (http://proteomecentral.proteomexchange.org) through the PRIDE partner repository with the dataset identifiers PXD010878 and PXD015454. The raw immunoblot images and files from statistical analyses are supplied as source data. Other raw and analyzed data files are available from the corresponding author upon reasonable request. A data availability statement is also included in the reporting summary linked to this article.

References

59. Lv, D.-W., Zhang, K. & Li, R. Interferon regulatory factor 8 regulates aspase-1 expression to facilitate Epstein–Barr virus reactivation in response to B cell receptor stimulation and chemical induction. *PLoS Pathog.* **14**, e1006868 (2018).
60. Wiśniewski, J. R. et al. Universal sample preparation method for proteome analysis. *Nat. Methods* **6**, 359–362 (2009).
61. Nesvizhskii, A. I., Keller, A., Kolker, E. & Aebersold, R. A statistical model for identifying proteins by tandem mass spectrometry. *Anal. Chem.* **75**, 4646–4658 (2003).
62. Tyanova, S. et al. The Perseus computational platform for comprehensive analysis of (prote) omics data. *Nat. Methods* **13**, 731–740 (2016).
63. Vizcaíno, J. A. et al. The PRoteomics IDEntifications (PRIDE) database and associated tools: status in 2013. *Nucleic Acids Res.* **41**, D1063–D1069 (2013).
64. US Food and Drug Administration. *Bioanalytical Method Validation, Guidance for Industry* (US Department of Health and Human Services Food and Drug Administration, 2018).

Acknowledgements

This study was supported by US National Institutes of Health (NIH) grants R01 CA211963 (D.Z.), R01 CA219836 (D.Z.), R01 GM109645 (R.H.), R01 CA205224 (R.H.), R01 CA200673 (W.Z.), R01 CA203834 (W.Z.), R21 CA223371 (G.Z.), R35 CA210065 (A.F.), R01 CA172809 (Y.-M.K.), Department of Defense grant BC180227 (W.Z.), the Schwab Charitable fund (M.K.) and CPRIT grant RP160716 (P.J.H.). Mass spectrometric support was provided by Alan J. Tackett and Samuel G. Mackintosh in the UAMS Proteomics Core Facility.

Author contributions

S.K. designed, performed and analyzed most of the experiments and wrote the manuscript; X.Z. designed, synthesized and analyzed BCL-X_L PROTACs and wrote the manuscript; D.L. designed, performed and analyzed the mass-spectrometry experiments, nanoBRET assay and wrote the manuscript; Y.H., D.T., J.S.W., J.P., W.Z., A.S., C.R.M, V.M.K., N.B., A. R. and G.H. performed and analyzed some experiments; P.Z and X.L. designed, synthesized and analyzed BCL-X_L PROTACs; A.A.F. and Y.-M.K. provided the PDX T-ALL model and revised the manuscript; Q.Z. and M.K. designed and performed the PDX T-ALL study and analyzed and interpreted data and revised the manuscript; Y.Y., P.J.H, W.Z. and R.H. interpreted data and revised the manuscript; G.Z. designed and supervised the study, analyzed and interpreted data and revised the manuscript. D.Z. conceived, designed and supervised the study, analyzed and interpreted data, and wrote the manuscript. All authors discussed the results and commented on the manuscript.

Competing interests

S.K., X.Z, Y.H., P.Z., G.Z. and D.Z. are inventors of two pending patent applications for use of BCL-X_L PROTACs as senolytic and antitumor agents. R.H., G.Z. and D.Z. are co-founders of and have equity in Dialectic Therapeutics, which develops BCL-X_L PROTACs to treat cancer.

Additional information

Extended data is available for this paper at https://doi.org/10.1038/s41591-019-0668-z.

Supplementary information is available for this paper at https://doi.org/10.1038/s41591-019-0668-z.

Correspondence and requests for materials should be addressed to G.Z. or D.Z.

Peer review information Javier Carmona was the primary editor on this article and managed its editorial process and peer review in collaboration with the rest of the editorial team

Reprints and permissions information is available at www.nature.com/reprints.

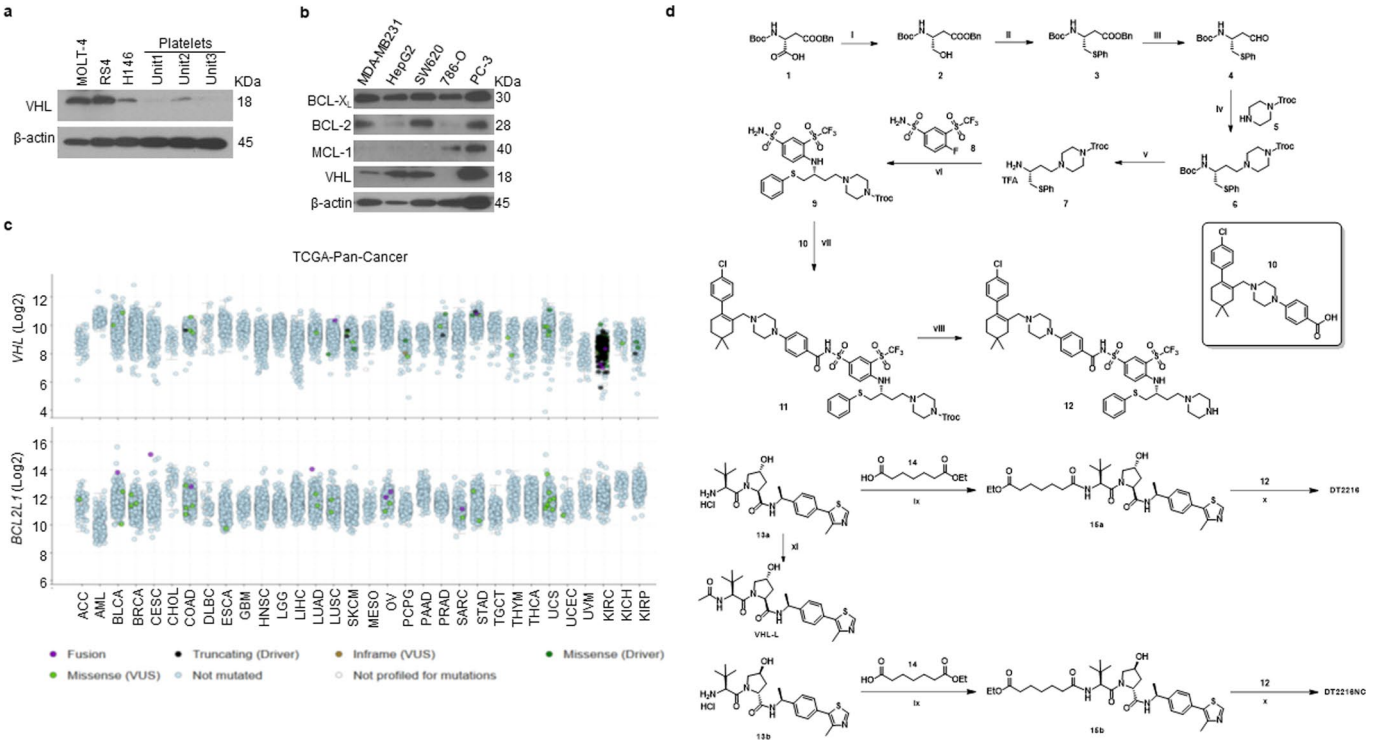

Extended Data Fig. 1 | Expression of anti-apoptotic BCL-2 members and VHL in cancer, and the synthetic schemes of DT2216 and DT2216NC. a, A representative of three immunoblot analyses of VHL in three different human tumor cell lines and platelets from three different individuals (indicated as units 1–3). **b**, Immunoblot analyses of the basal protein levels of BCL-X_L, BCL-2, MCL-1 and VHL in different solid tumor cells. Data are representative of two independent experiments. **c**, *BCL2L1* and *VHL* mRNA expression (log_2 transformed) and mutational status were analyzed using TCGA PanCancer Atlas studies via cBioPortal. **d**, Synthetic schemes of DT2216, DT2216NC and VHL-L. Reagents and conditions: (i) (1) *N*-methylmorpholine, isobutyl chloroformate, THF, −25 °C then −15 °C; (2) $NaBH_4$, H_2O, −15 °C; (ii) Bu_3P, diphenyl disulfide, toluene, 80 °C; (iii) DIBAL-H, toluene, −78 °C (iv) compound 5, $NaBH(OAc)_3$, TEA, DCM; (v) TFA, DCM; (vi) compound 8, TEA, acetonitrile, reflux; (vii) compound 10, EDCI, DMAP, DCM; (viii) Zn, HOAc, THF; (ix) HATU, TEA, DCM; (x) (1) LiOH monohydrate, methanol, H_2O; (2) compound 12, HATU, TEA, DCM; (xi) Ac_2O, TEA, DCM.

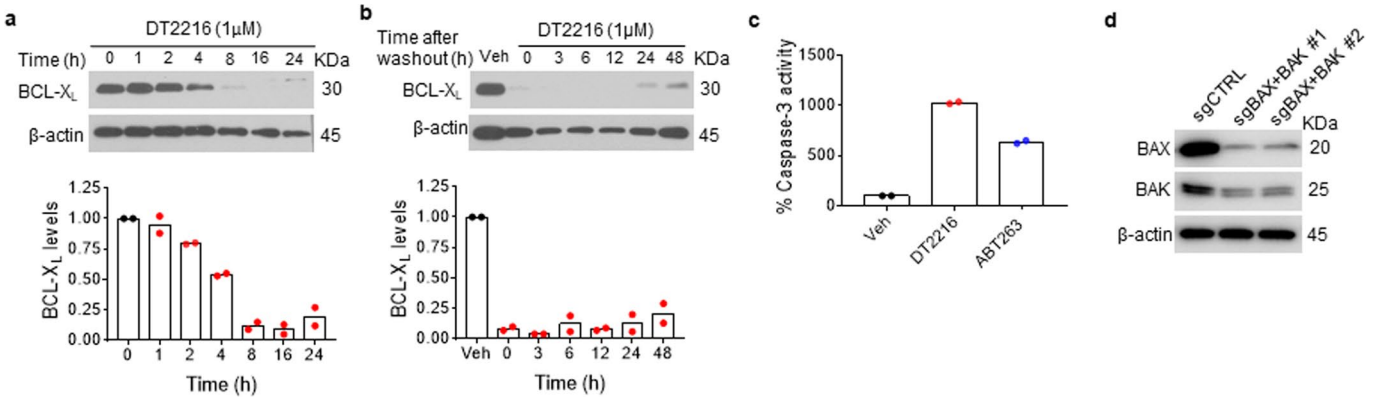

Extended Data Fig. 2 | The BCL-X_L degradation by DT2216 is rapid and long lasting. a, Immunoblot analysis of BCL-X_L expression in MOLT-4 cells after they were treated with DT2216 for various durations as indicated. A representative immunoblot is presented on the top panel. Densitometric analysis of BCL-X_L expression is presented on the bottom panel as mean of two independent experiments. Each symbol represents data (% of 0 h) from an individual experiment. **b**, Analysis of BCL-X_L expression by immunoblot in MOLT-4 cells treated with DT2216 for 16 h followed by drug withdrawal and then cultured without DT2216 for 0 to 48 h as indicated. A representative immunoblot is on the top panel. Densitometric analysis of BCL-X_L expression is presented on the bottom panel as the mean of two independent experiments. Each symbol represents data (% of Veh) from an individual experiment. **c**, Caspase-3 activity in MOLT-4 cells was measured 24 h after they were treated with 1 μM of DT2216 or ABT263. Data are presented as the mean ($n = 2$ technical replicates) of a representative experiment. Each symbol represents data (% of Veh) from an individual replicate. Similar results were obtained in an additional independent experiment. **d**, Representative immunoblot to confirm CRISPR–Cas9-mediated double knockout of *BAX* and *BAK* in H146 cells. The experiment was repeated independently one more time with similar results.

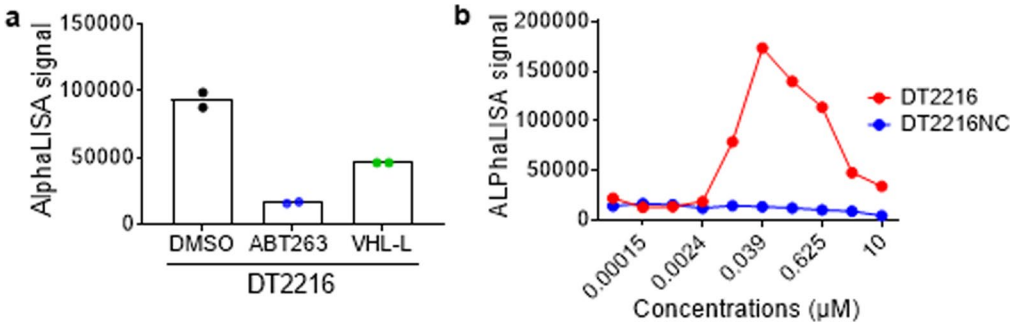

Extended Data Fig. 3 | ABT263 or VHL-L blocks the formation of ternary complex of BCL-X_L, DT2216 and VHL. a, Recombinant His-tagged BCL-X_L protein (100 nM) was incubated with the VHL-Elongin B/C complex (50 nM) with 0.039 μM of DT2216. The ternary complex formation was abrogated in the presence of ABT263 (1 μM) or VHL-L (10 μM). Data are expressed as mean ($n = 2$ technical replicates). Each symbol represents data from an individual replicate. **b**, The negative-control of DT2216 (DT2216NC) cannot form a ternary complex with BCL-X_L and the VHL complex. Recombinant His-tagged BCL-X_L protein (100 nM) was incubated with the VHL-Elongin B/C complex (50 nM) with increasing concentrations of DT2216 or DT2216NC. Data are expressed as mean ($n = 2$ technical replicates).

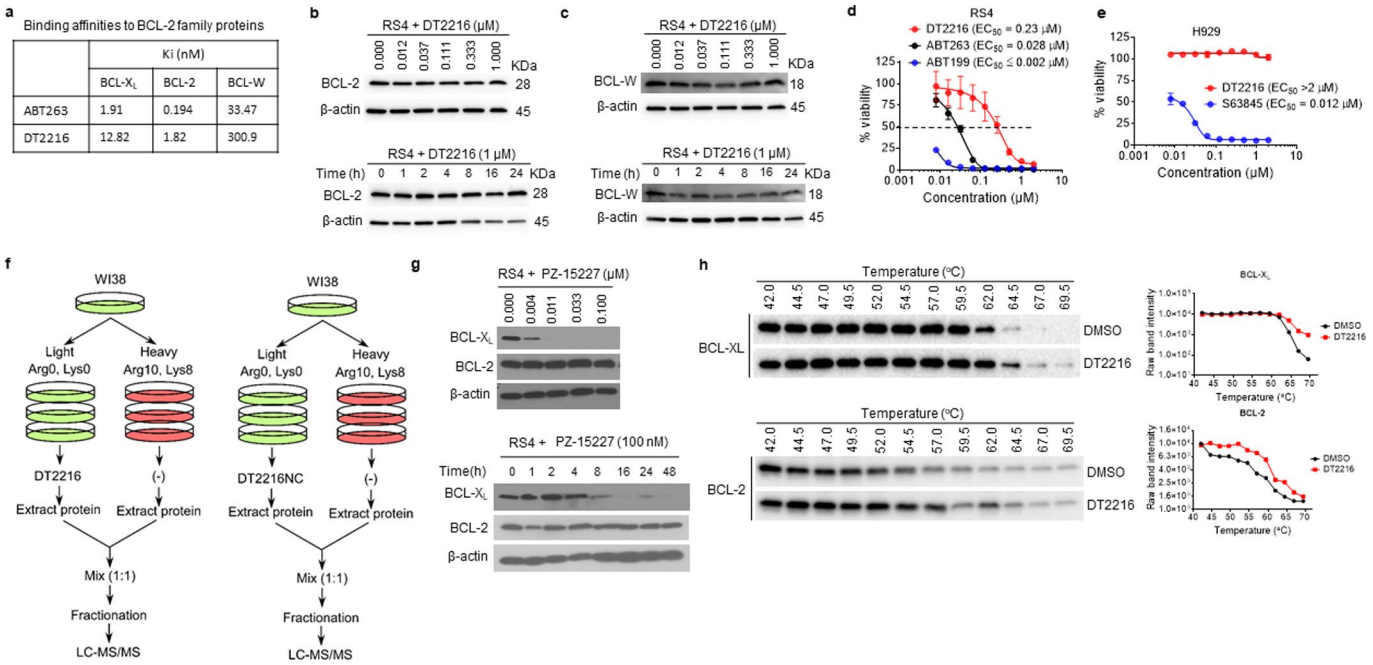

Extended Data Fig. 4 | DT2216 binds to both BCL-X_L and BCL-2 but cannot degrade BCL-2. a, The binding affinities of DT2216 and ABT263 towards BCL-X_L, BCL-2 and BCL-W were measured by AlphaScreen and are represented in terms of inhibition constant (K_i). The data are average of two independent experiments each performed in duplicates. **b**,**c**, Immunoblot analyses of BCL-2 and BCL-W are shown after the RS4 cells were treated with indicated concentrations of DT2216 for 16 h (top), or with 1 μM of DT2216 for indicated durations (bottom). **d**, Cell viability of BCL-2-dependent RS4 cells after treatment with increasing concentrations of DT2216, ABT199 or ABT263 for 72 h. Data are presented as mean ± s.d. from six replicate cell cultures in one experiment. Similar results were obtained in two additional independent experiments for DT2216. The EC_{50} of DT2216 is the average of three independent experiments. **e**, Cell viability of MCL-1-dependent H929 cells after treatment with increasing concentrations of DT2216 or S63845 for 72 h. Data are presented as mean ± s.d. from six replicate cell cultures in one experiment. **f**, Schematic representation of the proteomic assay shown in Fig. 3c. **g**, Representative immunoblot analyses are shown after the cells were treated with indicated concentrations of PZ-15227 for 16 h (top) or with 0.1 μM of PZ-15227 for indicated time points (bottom). Similar results were obtained in one more independent experiment. **h**, CETSA assay for BCL-X_L and BCL-2. MOLT-4 (for BCL-X_L) or RS4 (for BCL-2) cells were treated with DMSO, or 1 μM of DT2216 for 6 h. Raw band intensities are mean of two independent experiments.

a DT2216 stability in mouse blood and plasma

Compound ID	Time (h)	Blood	Plasma	% remaining @ 1hr in blood	Blood / Plasma
Verapamil (control)	0	5.01E+01			
		5.26E+01			
	1	6.19E+01	5.68E+01	0.929	0.922
		4.87E+01	6.31E+01		
DT2216	0	1.11E+00			
		1.12E+00			
	1	1.32E+00	1.00E+00	0.885	1.25
		1.20E+00	1.01E+00		

b DT2216 liver microsomal stability

Species	Compound	% Remaining			
		0 min	15 min	30 min	60 min
Human	Verapamil	100.0	43.0	15.8	3.7
	DT2216	100.0	97.0	105.0	104.1
Dog	Verapamil	100.0	34.6	15.5	3.3
	DT2216	100.0	97.8	99.2	97.7
Rat	Verapamil	100.0	9.8	1.4	0.1
	DT2216	100.0	95.6	96.1	92.5

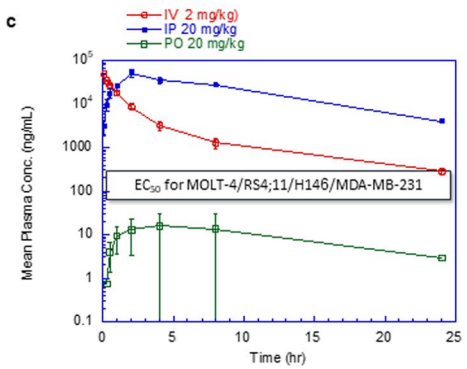

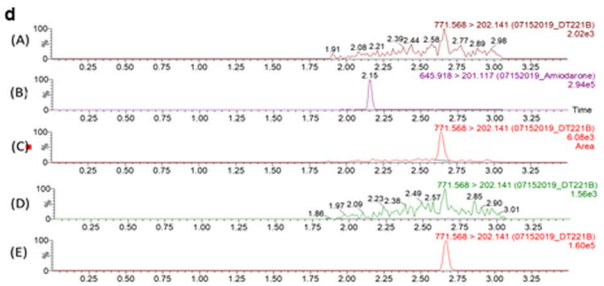

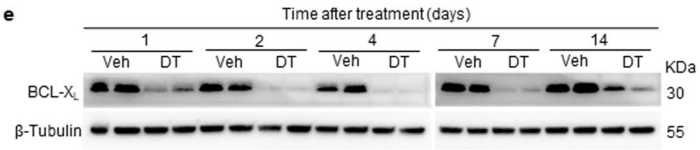

Extended Data Fig. 5 | Drug metabolism and pharmacokinetic/pharmacodynamic profile of DT2216. a, DT2216 stability in mouse blood and plasma. **b**, DT2216 liver microsomal stability. **c**, Plasma concentrations of DT2216 after a single administration of 2 mg per kg body weight (i.v. injection), 20 mg per kg body weight (i.p. injection) or 20 mg per kg body weight (p.o. administration) are presented as mean ± s.d. ($n = 3$ mice per group). These studies were done by BioDuro, a global contract research organization, through a contract. **d**, MRM chromatograms of (A) DT2216 in drug-free brain homogenate, (B) internal standard in spiked drug-free tumor homogenate (40 ng ml^{-1}), (C) DT2216 in spiked tumor homogenate (5 ng ml^{-1}; LLOQ), (D) DT2216 in tumor sample taken from vehicle dosed mouse at 24 h and (E) DT2216 in tumor sample taken at 24 h after 15 mg per kg body weight, i.p. administration. **e**, Representative immunoblot analysis of BCL-X_L in tumors at different durations after DT2216 (DT, 15 mg per kg body weight, i.p.) administration ($n = 2$ mice in vehicle and DT2216 groups at each time points). Similar results were obtained in two more immunoblot experiments.

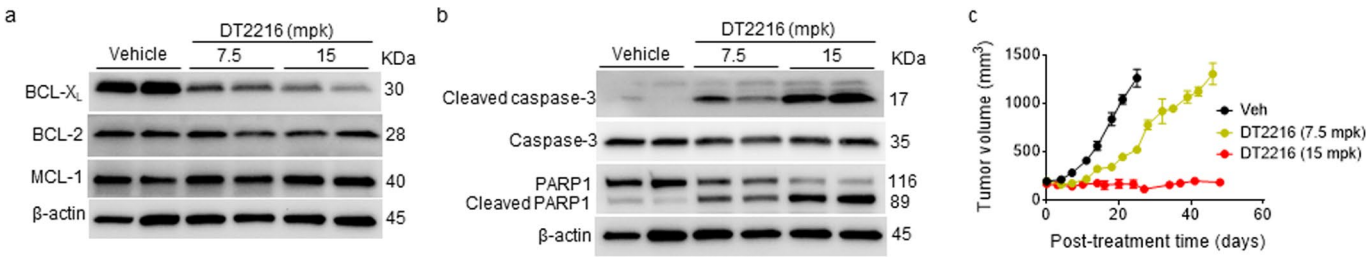

Extended Data Fig. 6 | DT2216 induces BCL-X_L degradation and apoptosis in MOLT-4 T-ALL xenografts and suppresses their growth in a dose-dependent manner. a,**b**, T-ALL xenograft tumors were collected 2 d after female CB-17 SCID mice received 1 i.p. injection of DT2216 at 7.5 mg per kg body weight and 15 mg per kg body weight. A single immunoblot analysis of BCL-X_L, BCL-2, MCL-1, cleaved and full length caspase-3 and PARP1 in the tumors is shown. **c**, Changes in tumor volume over time after the start of treatment with vehicle (Veh), or DT2216 (7.5 or 15 mg per kg body weight, q7d, i.p.). All the data presented are mean ± s.e.m. ($n = 8$ mice in vehicle, 8 mice in 7.5 mg DT2216 per kg body weight and 7 mice in 15 mg DT2216 per kg body weight). The data from the 15 mg DT2216 per kg body weight group are also presented in Extended Data Fig. 8f, in which the tumor size in these mice were continuously monitored till day 55 post-treatment.

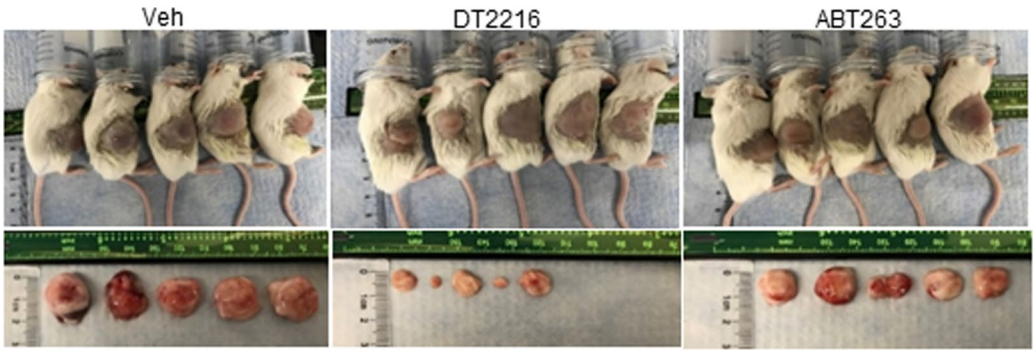

Extended Data Fig. 7 | Images of MOLT-4-tumor-bearing mice and excised tumors. The images shown (quantification data are shown in Fig. 4f,g) were captured at the end of the experiment, when the mice were treated with vehicle, DT2216 (15 mg per kg body weight, q7d, i.p.) or ABT263 (50 mg per kg body weight, qd, p.o.). The tumor-bearing mice (shown in the top) and harvested tumors (shown in the bottom) are not placed in an identical order.

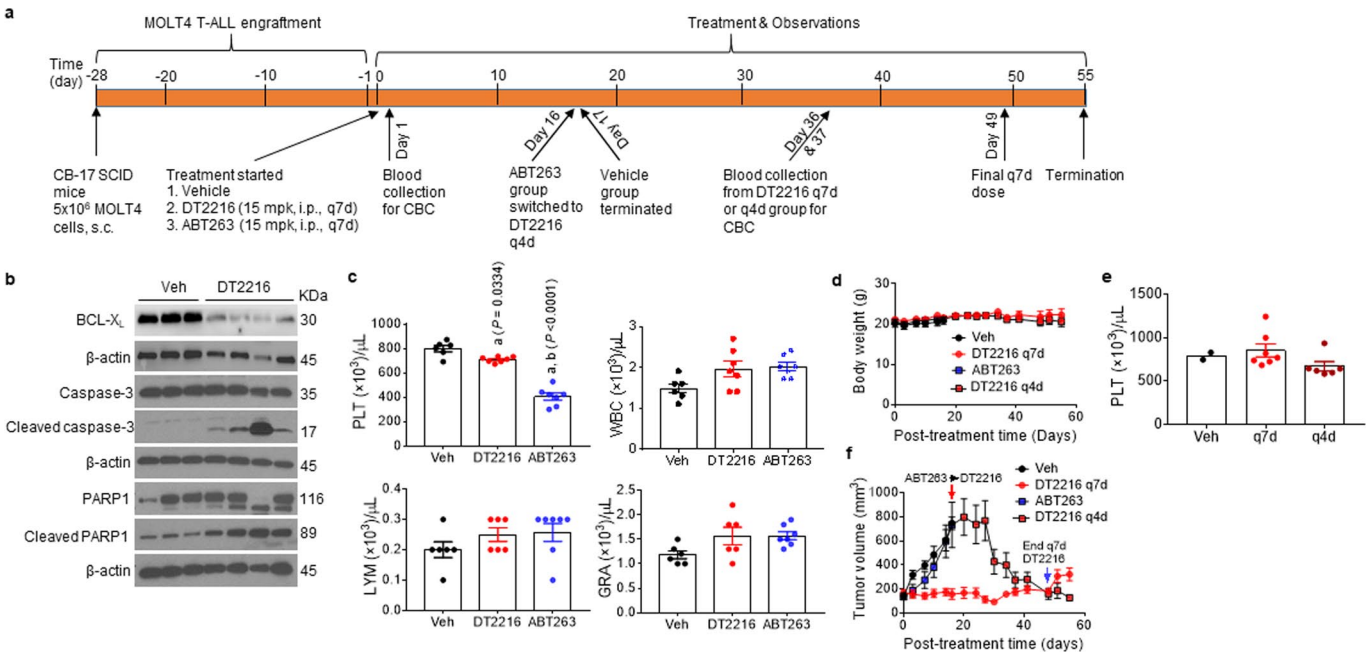

Extended Data Fig. 8 | DT2216 induces regression of MOLT-4 xenografts without causing thrombocytopenia. a, Illustration of the experimental design of the MOLT-4 T-ALL xenograft mouse model. **b**, Blots that are representative of two independent immunoblot analyses of BCL-X_L, cleaved and full-length caspase-3 and PARP1 in MOLT-4 T-ALL collected 2 d after tumor-bearing mice were treated with a single injection of vehicle or DT2216 (15 mg per kg body weight, i.p.). **c**, Blood platelets (PLT), white blood cells (WBC), lymphocytes (LYM) and granulocytes (GRA) were numerated 1 d after first treatment with vehicle, DT2216 (15 mg per kg body weight, i.p.) or ABT263 (15 mg per kg body weight, i.p.) as shown in **a**. *a* and *b* represent statistical significance versus Veh and DT2216, respectively, determined by one-way ANOVA and Tukey's multiple-comparison test. **d**, Body-weight changes in mice after the start of treatment with vehicle, DT2216 or ABT263 as shown in **a**. **e**, Numeration of PLT 1 d after the sixth dose of DT2216 (15 mg per kg body weight, q7d, i.p. or 15 mg per kg body weight, q4d, i.p.). Data are presented as mean ± s.e.m. ($n = 2$ mice in vehicle, 7 mice in DT2216 q7d and 6 mice in DT2216 q4d). **f**, Changes in tumor volume over time after the start of treatment with vehicle, DT2216 or ABT263 as shown in **a**. Data presented in **c**, **d** and **f** are mean ± s.e.m. ($n = 6$ mice for vehicle group and 7 mice each for DT2216 and ABT263 groups). Each symbol in **c** and **e** represents data from an individual animal.

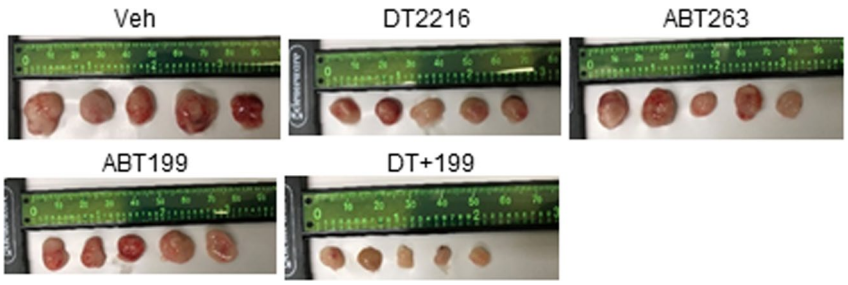

Extended Data Fig. 9 | Images of excised H146 SCLC tumors. The tumor images shown for the quantification data presented in Fig. 5g. Mice were treated as shown in Fig. 5c.

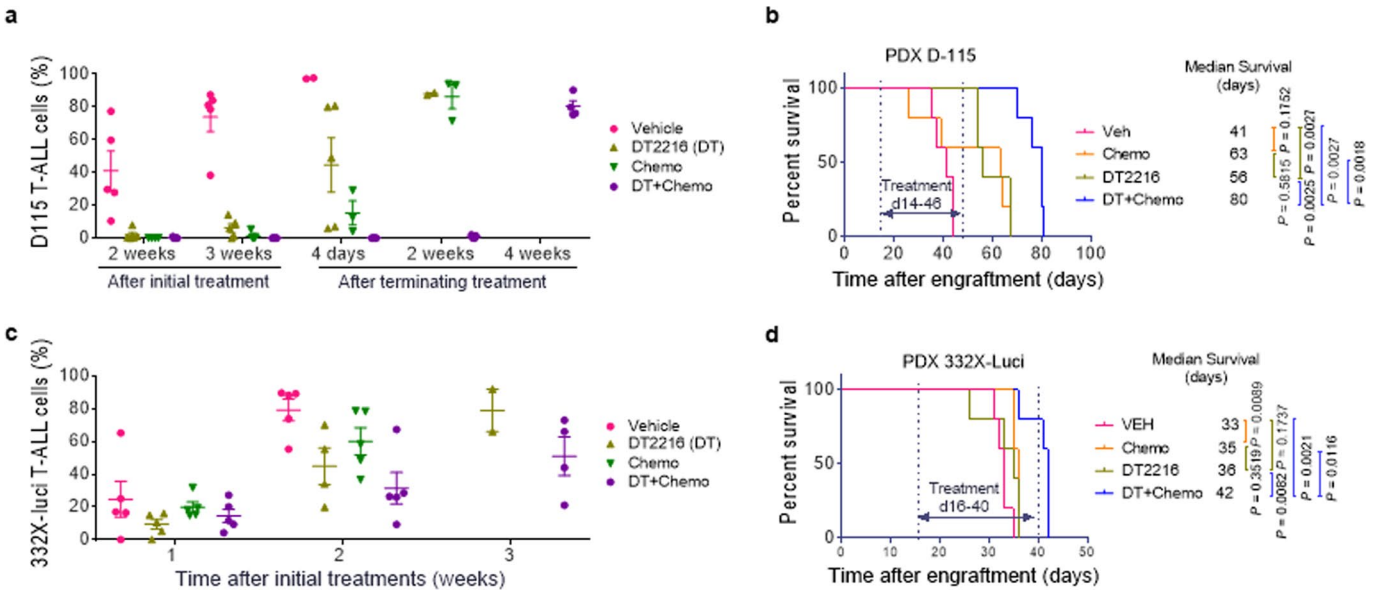

Extended Data Fig. 10 | Anti-leukemic activity of DT2216 alone and in combination with chemotherapy in T-ALL PDX models. a, Eight-week-old female NSG mice ($n = 20$ mice) were injected with 1×10^6 D115 cells 24 h after 0.25-Gy irradiation. Upon engraftment, mice were randomized to receive vehicle, DT2216 (15 mg per kg body weight, i.p., q4d for 3 weeks), chemotherapy (Chemo (vincristine 0.15 mg per kg body weight + dexamethasone 5 mg per kg body weight + L-asparaginase 1,000 units per kilogram body weight, i.p., q7d for 3 weeks)), or the combination of DT2216 with chemotherapy. Disease burden was followed by engraftment in bone marrow by checking hCD45% in bone marrow aspiration samples through flow cytometry. Data are presented as mean ± s.e.m. ($n = 5$ mice in each group). Each symbol represents data from an individual animal, and the middle horizontal line represents the mean. **b**, Mice survival was followed and statistical significance was determined by log-rank test ($n = 5$ mice in each group). **c**, Eight-week-old female NSG mice ($n = 20$ mice) were injected with 1×10^6 332X-luci cells 24 h after 0.25-Gy irradiation. Upon engraftment, mice were randomized to receive vehicle, DT2216, chemotherapy or the combination of DT2216 with chemotherapy as mentioned in **a**. Disease burden was followed by checking hCD45% in peripheral blood samples (retro orbital) through flow cytometry. Data are presented as mean ± s.e.m. ($n = 5$ mice in each group). Each symbol represents data from an individual animal, and the middle horizontal line represents the mean. **d**, Mice survival was followed, and statistical significance was determined by log-rank test ($n = 5$ mice in each group).

nature research

Corresponding author(s): Daohong Zhou

Last updated by author(s): 10-25-2019

Reporting Summary

Nature Research wishes to improve the reproducibility of the work that we publish. This form provides structure for consistency and transparency in reporting. For further information on Nature Research policies, see Authors & Referees and the Editorial Policy Checklist.

Statistics

For all statistical analyses, confirm that the following items are present in the figure legend, table legend, main text, or Methods section.

n/a	Confirmed	
☐	☒	The exact sample size (*n*) for each experimental group/condition, given as a discrete number and unit of measurement
☐	☒	A statement on whether measurements were taken from distinct samples or whether the same sample was measured repeatedly
☐	☒	The statistical test(s) used AND whether they are one- or two-sided *Only common tests should be described solely by name; describe more complex techniques in the Methods section.*
☐	☒	A description of all covariates tested
☒	☐	A description of any assumptions or corrections, such as tests of normality and adjustment for multiple comparisons
☐	☒	A full description of the statistical parameters including central tendency (e.g. means) or other basic estimates (e.g. regression coefficient) AND variation (e.g. standard deviation) or associated estimates of uncertainty (e.g. confidence intervals)
☐	☒	For null hypothesis testing, the test statistic (e.g. *F*, *t*, *r*) with confidence intervals, effect sizes, degrees of freedom and *P* value noted *Give P values as exact values whenever suitable.*
☒	☐	For Bayesian analysis, information on the choice of priors and Markov chain Monte Carlo settings
☒	☐	For hierarchical and complex designs, identification of the appropriate level for tests and full reporting of outcomes
☒	☐	Estimates of effect sizes (e.g. Cohen's *d*, Pearson's *r*), indicating how they were calculated

Our web collection on statistics for biologists contains articles on many of the points above.

Software and code

Policy information about availability of computer code

Data collection	Image Lab Touch version 2.2.0.08 Software (Bio-rad, Hercules, CA, USA) was used for scanning some of the immunoblots on the ChemiDoc MP imaging system; Gen5 version 3.04 software (BioTek, Winooski, VT, USA) was used for absorbance, fluorescence and luminescence measurements on Synergy Neo2 multi-mode plate reader; FlowJo V10 software was used for the acquisition of flow cytometry data; MassLynx and TargetLynx XS version 4.2 software (Waters, Milford, MA, USA) was used for data acquisition and quantification to determine DT2216 concentration in tumor samples.
Data analysis	ImageJ version 1.52a software (NIH) was used for the quantification of immunoblots; GraphPad Prism version 7 (GraphPad Software, La Jolla, CA, USA) was used for the preparation of all the graphs, determination of half maximal effective concentration (EC50) values, Inhibition constant (Ki), and the statistical analyses; Compusyn version 1.0 software (http://www.combosyn.com) was used for the determination of combination index (CI); MaxQuant version 1.6.2.10 software (https://maxquant.org/maxquant/) was used for the analysis of mass spectrometry data; FlowJo V10 software was used to analyze the flow cytometry data; Perseus version 1.6.8.0 software (https://maxquant.org/perseus/) was used for the statistical analysis of proteomics data; Scaffold version 4.10.0 (Proteome Software, Portland, OR, USA) was used to verify MS/MS based peptide and protein identifications; Phoenix WinNonlin version 6.1 (Certara, Princeton, NJ, USA) was used for the calculation of pharmacokinetic parameters presented in Table-4.

For manuscripts utilizing custom algorithms or software that are central to the research but not yet described in published literature, software must be made available to editors/reviewers. We strongly encourage code deposition in a community repository (e.g. GitHub). See the Nature Research guidelines for submitting code & software for further information.

Data

Policy information about availability of data

All manuscripts must include a data availability statement. This statement should provide the following information, where applicable:

- Accession codes, unique identifiers, or web links for publicly available datasets
- A list of figures that have associated raw data
- A description of any restrictions on data availability

The Mass Spectrometry (MS) data have been deposited to the ProteomeXchange Consortium (http://proteomecentral.proteomexchange.org) through the PRIDE partner repository with the dataset identifiers PXD010878 and PXD015454. These data have been released for public access. The raw immunoblot images and statistics data are supplied as source data linked with this article. Raw densitometric analyses files and plate-reader data files are available from the corresponding author upon reasonable request.

Field-specific reporting

Please select the one below that is the best fit for your research. If you are not sure, read the appropriate sections before making your selection.

☒ Life sciences ☐ Behavioural & social sciences ☐ Ecological, evolutionary & environmental sciences

For a reference copy of the document with all sections, see nature.com/documents/nr-reporting-summary-flat.pdf

Life sciences study design

All studies must disclose on these points even when the disclosure is negative.

Sample size	In our own experience 5-10 animals are sufficient to observe significant differences among different groups. For in vivo platelet toxicity studies, we used three animals in each group because the effect of treatments on platelet counts was consistent among different animals in a group. For PDX studies, the number of animals were based on sample availability and experimental feasibility. In other experiments, sample sizes were determined on the basis of previous studies that had used similar sample sizes to successfully determine a difference between groups. No statistical methods were used to predetermine sample sizes.
Data exclusions	In general, no data were excluded from the analyses unless there were obvious technical reasons. For example, in two samples the blood got clotted, hence could not be used for CBCs. One animal was excluded because of unsuccessful tumor engraftment.
Replication	Adequate measures were taken to verify the reproducibility of findings. An effect was confirmed across multiple cell lines and tumor samples with independent experiments and using several biological and technical replicates. The compounds were tested at multiple concentrations in vitro and the in vivo results were confirmed in different model systems such as cell line- and patient-derived xenografts. Some results were confirmed by different investigators and in different laboratory conditions. All attempts at replication were successful.
Randomization	Animals were randomized in different groups on the basis of tumor volumes in a way that each group had nearly equal average tumor volume at the start of treatment.
Blinding	Investigators were not blinded during randomizing the mice in different groups. Blinding was not possible because the animals were segregated into separate labeled cages with nearly equal average tumor volumes in each treatment group. When randomizing the animals in different treatment groups, the animals with lowest tumor sizes were first assigned to each group and so on to ensure that each group had animals with similar tumor sizes.

Reporting for specific materials, systems and methods

We require information from authors about some types of materials, experimental systems and methods used in many studies. Here, indicate whether each material, system or method listed is relevant to your study. If you are not sure if a list item applies to your research, read the appropriate section before selecting a response.

Materials & experimental systems

n/a	Involved in the study
☐	☒ Antibodies
☐	☒ Eukaryotic cell lines
☒	☐ Palaeontology
☐	☒ Animals and other organisms
☒	☐ Human research participants
☒	☐ Clinical data

Methods

n/a	Involved in the study
☒	☐ ChIP-seq
☐	☒ Flow cytometry
☒	☐ MRI-based neuroimaging

Antibodies

Antibodies used

For immunoblotting: the rabbit polyclonal VHL (Cat. No. 68547S, dilution 1:1000), BCL-XL (Cat. No. 2762S, dilution 1:2000), caspase-3 (Cat. No. 9662S, dilution 1:1000), cleaved Caspase-3 (clone Asp175, Cat. No. 9661S, dilution 1:1000), cleaved PARP1 (clone Asp214, Cat. No. 9541S, dilution 1:1000), Flag tag (Cat. No. 2044S, dilution 1:1000), BAX (Cat. No. 2772S, dilution 1:1000), and β-tubulin (Cat. No. 2146S, dilution 1:5000); the rabbit monoclonal MCL-1 (clone D35A5, Cat. No. 5453S, dilution 1:1000), BCL-2 (clone 50E3, Cat. No. 2870S, dilution 1:500), BCL-W (clone 31H4, Cat. No. 2724S, dilution 1:500), PARP1 (clone 46D11, Cat. No. 9532S, dilution 1:1000), BAK (clone D4E4, Cat. No. 12105S, dilution 1:1000), BIM (clone C34C5, Cat. No. 2933S, dilution 1:1000), PUMA (clone D30C10, Cat. No. 12450S, dilution 1:1000), HA tag (clone C29F4, Cat. No. 14031S, dilution 1:1000), and β-actin (clone 13E5, Cat. No. 4970L, dilution 1:5000) were purchased from Cell Signaling Technology. The mouse monoclonal β-actin (clone C4, Cat. No. 8691001, dilution 1:10000) was purchased from MP Biomedicals. The goat anti-rabbit (Cat. No. 7074S, dilution 1:3000) and horse anti-mouse (Cat. No. 7076S, dilution 1:3000) HRP-conjugated secondary antibodies were purchased from Cell Signaling Technology. The goat anti-rabbit IgG, Fc fragment specific (Cat. No. 111-035-046, dilution 1:10000) was purchased from Jackson ImmunoResearch.
For immunoprecipitation: the mouse monoclonal BCL-XL (clone 7B2.5, Cat. No. sc-56021, dilution 1:50) and normal mouse IgG (Cat. No. sc-2025, dilution 1:100) were purchased from Santa Cruz Biotechnology.
For flow cytometry: the rat IgG2b, κ, APC mCD45-APC (clone 30-F11, Cat. No. 103111, dilution 1:250) and Mouse IgG1, κ, FITC hCD45-FITC (clone H130, Cat. No. 304038, dilution 1:250) were purchased from Biolegend.

Validation

All the used antibodies are commercially available. The antibodies used in a specific species or application have been validated by manufacturers to be used in that species/application and this information is provided in their website and/or antibody datasheets.

Eukaryotic cell lines

Policy information about cell lines

Cell line source(s)

All the cell lines were purchased from American Type Culture Collection (ATCC), except EJM and NCI-H929 cells which were kind gift from Dr. Erming Tian at the Winthrop P. Rockefeller Cancer Institute at University of Arkansas for Medical Sciences. MOLT-4 (ATCC, Cat. No. CRL-1582); RS4;11 (ATCC, Cat. No. CRL-1873); NCI-H146 (ATCC, Cat. No. HTB-173); MDA-MB-231 (ATCC, Cat. No. HTB-26); PC-3 (ATCC, Cat. No. CRL-1435); HepG2 (ATCC, Cat. No. HB-8065); SW620 (ATCC, Cat. No. CCL-227); 786-O (ATCC, Cat. No. CRL-1932); WI-38 (ATCC, Cat. No. CCL-75); HEK 293T (ATCC, Cat. No. ACS-4500).

Authentication

The cell lines have been validated by the suppliers. The morphology and growth of the used cell lines were verified with the supplier's data sheets, and their pharmacological responses were matched with the available literature.

Mycoplasma contamination

Cell lines were recently purchased from ATCC and were not further tested for mycoplasma contamination in our laboratory.

Commonly misidentified lines
(See ICLAC register)

NCI-H929 was used to generate some supporting data (Fig 3a, b and supplemetary Fig. 4e). This cell line is known to solely depend on MCL-1 for their survival and has also been previously used for this purpose (Kotschy, A. et al. Nature. 2016, 538, 477–482). The data pertaining to this cell line does not have any significant impact on the outcomes of our study. None of the other cell lines used are listed in ICLAC database.

Animals and other organisms

Policy information about studies involving animals; ARRIVE guidelines recommended for reporting animal research

Laboratory animals

Female CB17/Icr-Prkdcscid/IcrIcoCrl (CB-17 SCID), CB17.Cg-PrkdcscidLystbg-J/Crl (CB-17 SCID-beige), or NOD.CB17-Prkdcscid/NCrCrl (NOD-SCID) mice aged 5-6 weeks were purchased from Charles River Laboratories. Female NOD-scid IL2Rgnull (NSG) mice aged 6-7 weeks were purchased from Jackson Laboratory.

Wild animals

The study did not involve wild animals.

Field-collected samples

The study did not involve samples collected from the field.

Ethics oversight

All animal work was approved and done in accordance with the Institutional Animal Care and Use Committees of University of Arkansas for Medical Sciences, University of Florida, and MD Anderson Cancer Center with the exception of the pharmacokinetic (PK) studies that were done by BioDuro (San Diego, CA, USA), a global contract research organization, through a contact. All animal studies were complied with the ethical regulations and humane endpoint according to the NIH Guidelines for the Care and Use of Laboratory Animals.

Note that full information on the approval of the study protocol must also be provided in the manuscript.

Flow Cytometry

Plots

Confirm that:

☒ The axis labels state the marker and fluorochrome used (e.g. CD4-FITC).

☒ The axis scales are clearly visible. Include numbers along axes only for bottom left plot of group (a 'group' is an analysis of identical markers).

☒ All plots are contour plots with outliers or pseudocolor plots.

☒ A numerical value for number of cells or percentage (with statistics) is provided.

Methodology

Sample preparation	Peripheral blood samples were collected through retro orbital bleeding, and red blood cells were lysed at room tempreture for 30 min. The samples were washed once with PBS, and stained in antibody cocktail for 15 min at room temperature. After washing with PBS, the samples were re-suspended in PBS plus DAPI and immediately analyzed by flow cytometry.
Instrument	Gallios, Beckman Coulter
Software	FlowJo, V10.
Cell population abundance	All samples were collected at least 50,000 events of live cells.
Gating strategy	FSC/SSC was used to distinguish the cell size. DAPI-negative was used to gate the live cells followed by mCD45 and hCD45 to gate mouse and human white blood cells, respectively.

☒ Tick this box to confirm that a figure exemplifying the gating strategy is provided in the Supplementary Information.